NEAR INFRARED INTERFERENCE FILTER DESIGN AND THE PRODUCTION WITH ION-ASSISTED DEPOSITION TECHNIQUES

A THESIS SUBMITTED TO
THE GRADUATE SCHOOL OF NATURAL AND APPLIED SCIENCES
OF
MIDDLE EAST TECHNICAL UNIVERSITY

BY

SELÇUK AYDOĞDU

IN PARTIAL FULFILLMENT OF THE REQUIREMENTS
FOR
THE DEGREE OF MASTER OF SCIENCE
IN
PHYSICS

FEBRUARY 2012

Approval of the thesis:

NEAR INFRARED INTERFERENCE FILTER DESIGN AND THE PRODUCTION WITH ION-ASSISTED DEPOSITION TECHNIQUES

submitted by **SELÇUK AYDOĞDU** in partial fulfillment of the requirements for the degree of **Master of Science in Physics Department, Middle East Technical University** by,

Prof. Dr. Canan Özgen ________________
Dean, Graduate School of **Natural and Applied Sciences**

Prof. Dr. Mehmet Tevfik Zeyrek ________________
Head of Department, **Physics**

Assoc. Prof. Dr. Akif Esendemir ________________
Supervisor, **Physics Dept., METU**

Examining Committee Members:

Prof. Dr. Mehmet Parlak
Physics Dept., METU ________________

Assoc. Prof. Dr. Akif Esendemir
Physics Dept., METU ________________

Assoc. Prof. Dr. Enver Bulur
Physics Dept., METU ________________

Assist. Prof. Dr. Sinan Kaan Yerli
Physics Dept., METU ________________

Dr. Ali Alaçakır
TAEK SANAEM ________________

Date: February 2012

I hereby declare that all information in this document has been obtained and presented in accordance with academic rules and ethical conduct. I also declare that, as required by these rules and conduct, I have fully cited and referenced all material and results that are not original to this work.

Name, Last name: Selçuk Aydoğdu

Signature :

ABSTRACT

NEAR INFRARED INTERFERENCE FILTER DESIGN AND THE PRODUCTION WITH ION-ASSISTED DEPOSITION TECHNIQUES

Aydoğdu, Selçuk
M.Sc., Department of Physics
Supervisor : Assoc. Prof. Dr. Akif Esendemir

February 2012, 67 pages

Near infrared region (NIR) of the electromagnetic spectrum (EM) is defined as 700nm to 1400nm wavelength interval by International Commission on Illumination(CIE). This wavelength interval is extensively used for target acquisition, night vision, wireless communication etc. Therefore, filtering the desired portion of EM spectra becomes a need for that kind of applications. Interference filters are multilayer optical devices which can be designed and produced for the desired wavelength intervals. The production of near infrared interference filters is a process of depositing thin material layers on the suitable substrates. In this thesis, a multilayer NIR filter will be designed for a selected wavelength interval by the use of different materials. Then, transmission quality, thermal stability, dependence of the transmission values on the incoming beam angle, performance and durability of the filter will be studied.

Keywords: Near Infrared interference filter, multilayer optical coatings, thin film deposition techniques, E-beam evaporation, Optilayer.

ÖZ

YAKIN KIZILÖTESİ GİRİŞİM FİLTRE TASARIMI VE İYON DESTEKLİ DEPOZİSYON YÖNTEMLERİ İLE ÜRETİMİ

Aydoğdu, Selçuk
Yüksek Lisans, Fizik Bölümü
Tez Yöneticisi : Doç. Dr. Akif Esendemir

Şubat 2012, 67 sayfa

Elektromanyetik spektrumun yakın kızılötesi bölgesi Uluslararası Aydınlatma Komisyonu (CIE) tarafından 700nm'den 1400nm'ye kadar ki dalgaboyu aralığı olarak tanımlanır. Bu dalgaboyu aralığı yaygın olarak hedef tespiti, gece görüşü, kablosuz iletişim vs gibi alanlarda yaygın olarak kullanılır. Sonuçta, elektromanyetik spektrumun istenilen bölümünü filtrelemek , bu tür uygulamalar için ihtiyaç haline gelmektedir. Girişim filtreleri, istenilen dalgaboyu aralığı için tasarlanabilen ve üretilebilen çok katmanlı optiksel araçlardır. Yakın kızılötesi girişim filtrelerinin üretimi uygun malzemelerin ince katmanlarının uygun alttaş üzerine biriktirilmesi işlemidir. Bu tez çalışmasında, farklı malzemeler kullanılarak, seçilen bir dalgaboyu aralığı için çok katmanlı bir yakın kızılötesi filtre tasarlanacaktır. Daha sonra filtrenin, geçirgenlik kalitesine, termal kararlığına, gelen ışın açısına bağlı olarak geçirgenlik performansı ve zamana karşı dayanıklılığı çalışılacaktır.

Anahtar Kelimeler: Yakın kızılötesi girişim filtresi , Çok katmanlı optik kaplamalar , İnce film biriktirme yöntemleri , Elektron demeti buharlaştırma , Optilayer.

To my family...

ACKNOWLEDGMENTS

I would like to thank my parents, Şerif and Meryem, for their love and support throughout my life. I also wish to thank my sister , Hicran, for being in my life.

I would like to express my appreciation to my supervisor Assoc. Prof. Dr. Akif Esendemir. I am grateful for his endless patience and his support.

I would also like to thank to my friends Ercan Aydın, Selim Kara, Duygu Kurulay, Engin Özören. They were always with me and they always gave me support morally.

Finally, I wish to give special thanks to Didem Kandil and Emir Kılıç for their friendness and support. To tell the truth, without their continuous support it would be impossible to complete this study.

TABLE OF CONTENTS

ABSTRACT iv

ÖZ v

ACKNOWLEDGMENTS vii

TABLE OF CONTENTS viii

LIST OF TABLES x

LIST OF FIGURES xii

CHAPTERS

1 INTRODUCTION 1

2 THEORY OF OPTICAL COATING 3

2.1 Introduction 3

2.2 Theory of Optical Thin Film 3

2.2.1 Single Layer Antireflective (AR) Coating 11

2.2.2 Two Layer Antireflective (AR) Coating 13

2.2.3 Three Layer Antireflective (AR) Coating 15

2.3 Reflective Coatings 17

2.3.1 Dielectric Mirrors 17

2.3.2 High Reflective Metallic Coatings 19

3 THIN FILM DEPOSITION TECHNIQUES 21

3.1 Introduction 21

3.2 Thin Film Deposition Methods 21

3.2.1 Chemical Vapor Deposition (CVD) 22

3.2.2 Physical Vapor Deposition (PVD) 22

3.2.2.1 Thermal Evaporation 23

3.2.2.2 Electron Beam Evaporation 23

3.2.2.3 Sputtering 26
3.2.2.4 Ion Assisted Deposition (IAD) and Plasma Ion Assisted Deposition (PIAD) 27
3.3 Optical Coating System 30
3.3.1 Evaporation Units 30
3.3.2 Advanced Plasma Source 32
3.3.3 Thickness Measurement Unit 33
3.3.4 Characterization 35
4 DESIGN AND PRODUCTION OF NEAR INFRARED INTERFERENCE FILTER 37
4.1 Introduction 37
4.2 Design of a Near Infrared Interference Filter 38
4.3 Homogeneity Studies 41
4.4 Production and Analysis of the Near Infrared Interference Filter with OMS 43
4.5 Production and Analysis of the Near Infrared Interference Filter with Quartz Crystal 52
4.6 Angle of Incidence Analysis 56
4.7 Durability Analysis 60
5 CONCLUSION 62
REFERENCES 64
APPENDICES
A THICKNESS DATA FOR THE PRODUCED FILTERS 65

LIST OF TABLES

TABLES

Table 2.1 Reflectance of Aluminum, Silver and Gold 20

Table 3.1 Evaporation Characteristics of coating Materials 25

Table 3.2 Comparison between Evaporation and Sputtering methods 27

Table 3.3 Camparison of Typical Thin Film Deposition Techniques 29

Table 3.4 APS Parameters 33

Table 3.5 Spectrophotometer specifications 36

Table 4.1 Average transmission value of the designed 31 layer NIR interference filter with backside reflections 41

Table 4.2 Average reflection values of the designed 31 layer NIR interference filter with back side reflections 49

Table 4.3 Average transmission values of the designed 31 layer NIR interference filter with back side antireflective coating design 50

Table 4.4 Average reflection values of the designed 31 layer NIR interference filter with back side antireflective coating design 51

Table 4.5 Average transmission values of the designed 27 layer NIR interference filter with back side antireflective coating design 53

Table 4.6 Average reflection values of the designed 27 layer NIR interference filter with back side reflections 54

Table 4.7 Average transmission values of the designed 27 layer NIR interference filter with backside antireflective coating design 56

Table 4.8 Transmission values of two samples after transmission and three months after production 61

Table 5.1 Transmission and thickness values of produced and designed NIR interference filters. 63

Table 5.2 Reflection and thickness values of produced and designed NIR interference filters. 63

Table A.1 Thickness data for the produced 27 layer NIR interference filters 65

Table A.2 Thickness data for the produced 31 layer NIR interference filters 66

Table A.3 Thickness data of antireflective backside coating for the produced filters . . 67

LIST OF FIGURES

FIGURES

Figure 2.1 Reflection on the thin film 4

Figure 2.2 Reflection end refraction of a beam from a single layer. 6

Figure 2.3 Reflection vs wavelength for single layer coatings designed with different refractive indices. 12

Figure 2.4 Antireflecting double layer using $\lambda/4 - \lambda/4$ and $\lambda/4 - \lambda/2$ thickness films. 14

Figure 2.5 Reflectance vs Wavelength for the double layer coating. (a) quarter-quarter wavelength; $n_1 = 1.65, n_2 = 2.1$. (b) quarter-half wavelength; $n_1 = 1.38, n_2 = 1.6$. (c) quarter-half wavelength; $n_1 = 1.38, n_2 = 1.85$. $n_s = 1.52, n_0 = 1.0$ for all cases. 15

Figure 2.6 Antireflecting triple layers using $\lambda/4 - \lambda/4 - \lambda/4$ and $\lambda/4 - \lambda/2 - \lambda/4$ . . 16

Figure 2.7 Reflectance vs wavelength for two different triple layer coating. (a) quarter-quarter-quarter wavelength ;$n_1 = 1.38$, $n_2 = 2.02$, $n_3 = 1.8$. (b)(b) quarter-half-quarter wavelength ; $n_1 = 1.38$, $n_2 = 2.2$, $n_3 = 1.7$. $n_0 = 1.0$, $n_s = 1.52$ and $\lambda = 550nm$ for two cases. 16

Figure 2.8 Reflectance vs Wavelength for three different dielectric mirrors.(a) $N = 2$ double layers. (b) $N = 6$ double layers.(c) $N = 2$ double layers with an additional high index layer. $n_0 = 1.0$, $n_s = 1.52$, $n_H = 2.35$, $n_L = 1.38$ and layers are quarter wavelength at $\lambda = 550$ nm. 18

Figure 2.9 Reflectance vs Wavelength for some materials. 19

Figure 3.1 Thermal Evaporation in a coating system 23

Figure 3.2 Electron Beam evaporation system 24

Figure 3.3 Ion Beam Assisted deposition 28

Figure 3.4 Setup of a Plasma Ion-Assisted Deposition 29

Figure 3.5 Optical Coating System 30

Figure 3.6 Electron beam evaporation unit 1 31
Figure 3.7 Electron beam evaporation unit 2 31
Figure 3.8 Thermal evaporation unit 32
Figure 3.9 Advanced plasma source 33
Figure 3.10 Optical Monitoring System 34
Figure 3.11 OMS and Quartz Crystal measuring unit 35
Figure 3.12 Spectrophotometer 35

Figure 4.1 Target values on the software 38
Figure 4.2 Light source database 38
Figure 4.3 Substrate database 39
Figure 4.4 Layer materials database 39
Figure 4.5 Initial design for NIR interference filter 40
Figure 4.6 Initial design after applying refinement 40
Figure 4.7 Transmission of designed 31 layer NIR interference filter with backside reflections 41
Figure 4.8 Optical Coating System 42
Figure 4.9 Substrate positions on the substrate holder 42
Figure 4.10 Reflection of single layer SiO_2 43
Figure 4.11 Substrate holder with homogeneity mask 43
Figure 4.12 Transmission of uncoated glass(B270) 44
Figure 4.13 Reflection of uncoated glass(B270) 44
Figure 4.14 Transmission of measured 31 layer NIR interference filter with backside reflections 45
Figure 4.15 Reflection of measured single layer SiO_2 45
Figure 4.16 Transmission of measured single layer TiO_2 47
Figure 4.17 Transmission of measured 31 layer NIR interference filter with backside reflections 48
Figure 4.18 Reflection of designed 31 layer NIR interference filter with backside reflections 49

Figure 4.19 Reflection of measured 31 layer NIR interference filter with backside reflections 49

Figure 4.20 Transmission of designed 31 layer NIR interference filter with backside antireflective coating design 50

Figure 4.21 Transmission of measured 31 layer NIR interference filter with backside antireflective coating 51

Figure 4.22 Reflection of designed 31 layer NIR interference filter with backside antireflective coating design 51

Figure 4.23 Reflection of measured 31 layer NIR interference filter with backside antireflective coating 52

Figure 4.24 Transmission of designed 27 layer NIR interference filter with backside reflections 53

Figure 4.25 Transmission of measured 27 layer NIR interference filter with backside reflections 53

Figure 4.26 Reflection of designed 27 layer NIR interference filter with backside reflections 54

Figure 4.27 Reflection of measured 27 layer NIR interference filter with backside reflections 55

Figure 4.28 Transmission of designed 27 layer NIR interference filter with backside antireflective coating design 55

Figure 4.29 Transmission of measured 27 layer NIR interference filter with backside antireflective coating 56

Figure 4.30 Transmission of designed 31 layer NIR interference filter with 5° angle of incidence 57

Figure 4.31 Transmission of designed 31 layer NIR interference filter with 10° angle of incidence 57

Figure 4.32 Transmission of designed 31 layer NIR interference filter with 30° angle of incidence 58

Figure 4.33 Transmission of designed 31 layer NIR interference filter with 45° angle of incidence 58

Figure 4.34 Transmission of designed 27 layer NIR interference filter with 5° angle of incidence 59
Figure 4.35 Transmission of designed 27 layer NIR interference filter with 10° angle of incidence 59
Figure 4.36 Transmission of designed 27 layer NIR interference filter with 30° angle of incidence 60
Figure 4.37 Transmission of designed 27 layer NIR interference filter with 45° angle of incidence 60
Figure 4.38 Transmission spectrum after three months 61

CHAPTER 1

INTRODUCTION

Optical filters are designed and produced in order to change and modify the reflection or transmission properties of a substrate surface. It is usually accepted that there are two types of optical filters depending on the physical principles. First one of these optical filters is the absorbing filters and the other one is the interference filters. Absorbing filters are based on wavelength-dependent absorption in some material like a glass dopant, pigment or semiconductor[1]. In these filters , absorbed light is transformed into heat. On the other hand, interference filters are more complicated and band region can be changeable more easily in comparison with absorbing filters. Interference based filters involve dielectric coatings. These coatings are used for not only dielectric mirrors but also for thin film polarizers and beam splitters. Moreover, designing interference based filters ,band pass filters, high and low pass filters, notch filters and edge filters can be easily produced.

When we look at the applications of thin films , we can see that thin film technology may appear in all areas of our lives. Some of the most used applications of thin films are single and multilayer metal electrical conductor films, optical films for transmission and reflection, decorative films, decorative and wear-resistant coatings, permeation barriers for moisture and gases, corrosion resistant films, electrically insulating layers for microelectronics, coating of engine turbine blades, coating of high strength steels to avoid hydrogen embrittlement, diffusion barrier layers for semiconductor metallization, magnetic films for recording, transparent electrical conductors, wear and erosion resistant (hard) coatings (tool coatings), dry film lubricants and thin-walled freestanding structures [2].

Theory of optical filter, or thin film, is based on interference phenomena. Interference phenomena is depend on forming a new wave by superposing of two different waves. As two

waves reflect from parallel surfaces they superpose and interfere with each other. If the reflected waves interfere constructively there is a phase difference between the reflected waves, if they interfere destructively there is not a phase difference. Phase difference is identified by optical path difference and refractive indices of surfaces.

When we investigate the history of thin film phenomenon we meet with Robert Boyle and Robert Hooke firstly. They clarified “Newton Rings” phenomenon. Thomas Young discovered principle of interference of light in 1801. Young’s contribution went largely unnoticed until the work of Augustin Fresnel, in 1816, helped to establish the wave theory of light [3]. After J. C. Maxwell explained “Maxwell Equations” that states the electromagnetic nature of light, the basic theory of thin film phenomenon is clarified. When the first Fabry-Perot interferometer was developed in 1899, thin film interference phenomenon could be shown practically.

In the present work, some different designs of near infrared interference filter which is also called “Cold Mirror“ and the production of these filters are going to be shown and explained. Designed and produced Near infrared interference filters reflect the visible wavelength that is between in the spectral region 400 nm - 700 nm and transmit near infrared wavelength that is between in the spectral region 700 nm - 1400 nm.

In chapter two, the theory of interference phenomenon is given. Reflection and transmission of single, double and three layer antireflective coatings are given. Also, dielectric mirrors and high reflective metallic coatings are discussed and explained.

In chapter three, thin film production techniques are given. Moreover, optical coating system that is used for the designed coatings is presented briefly.

All the experimental works for the production of near infrared interference filter are given with measurement results in the chapter four. Furthermore, design steps that are done with the help of a software are shown in this chapter.

In chapter five, the designs and results of the productions are discussed and conclusion is presented.

CHAPTER 2

THEORY OF OPTICAL COATING

2.1 Introduction

Thin film interference is a physical event which happens between two reflected light waves from the upper and lower surface of a boundary. This phenomenon is the result of interfering two reflected light waves and these reflected light waves form a new light wave. In this chapter, physical properties of this new light wave will be given and discussed. As a result, transmission, reflection, refractive index of the film medium, thickness of the film are going to be discussed.

2.2 Theory of Optical Thin Film

When light hits the surface of a thin film, some of the intensity is transmitted and some of the intensity is reflected at the medium. A thin film is a layer of material which has a thickness from nanometers to several micron range. As transmitted light strikes the below surface there will be again transmission and reflection. While finding the percentage of reflection and transmission Fresnel equations will be derived and used. There will be interference between the reflected light from upper and lower surfaces and depending on the difference of their phase interference becomes constructively or destructively. This difference is changed by some parameters which are the thickness of thin film, the angle of incident wave on the thin film and the refractive index of thin film. Moreover, there will be a 180° (π radians) phase shift between the reflected light waves depending on the refractive indices of the materials on either side of the boundary. If the refractive index of the medium the wave is in the presence is lower than the refractive index of the medium the wave is striking, the phase shift exists[4].

This means that if $n_1 < n_2$ (the light goes to from material 1 to material 2), then a phase shift will happen depending on reflection. As a result of this phase shift, dark and bright bands will be observed in the pattern of the light. In order to calculate the phase shift between the reflected light from the boundaries and determine the condition of interference we have to consider the optical path difference (OPD) of the reflected light.

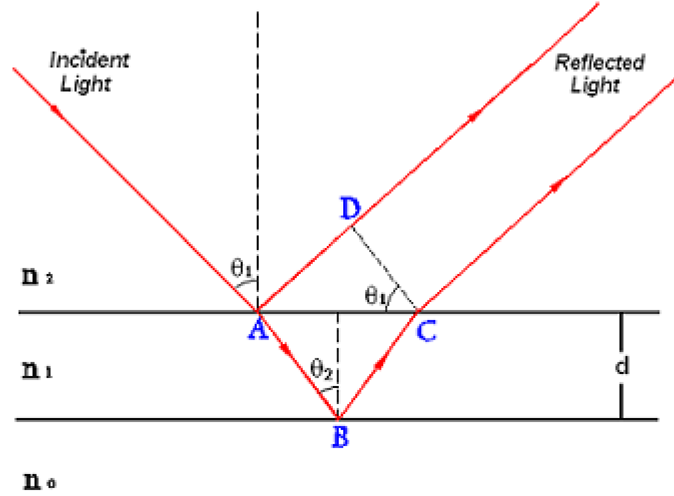

Figure 2.1: Reflection on the thin film

According to Figure 2.1, the OPD between the two waves is that:

$$\Delta = OPD = n_2(\overline{AB} + \overline{BC}) - n_1\overline{AD} \tag{2.1}$$

where,

$$(\overline{AB} = \overline{BC}) = \frac{d}{\cos\theta_2} \tag{2.2}$$

Using Snell's Law, $n_1.\sin\theta_1 = n_2.\sin\theta_2$

$$OPD = n_2\left(\frac{2d}{\cos\theta_2}\right) - 2d\tan\theta_2 n_2\sin\theta_2 \tag{2.3}$$

$$= 2n_2 d\left(\frac{1-\sin^2\theta_2}{\cos\theta_2}\right)$$

$$OPD = 2n_2 d\cos\theta_2 \tag{2.4}$$

The corresponding phase difference is $\delta = \triangle k = \triangle(\frac{2\pi}{\lambda})$. While calculating the net phase difference the possible phase difference from the reflection must be taken into account. As a

result, if we say optical path difference, $\triangle_p$, stated above equation 2.4 and equivalent path difference, $\triangle_r$, coming from phase change on reflection, we can indicate the conditions for constructive and destructive interferences.

Constructive interference : $\triangle = \triangle_p + \triangle_r = m\lambda$

Destructive interference : $\triangle = \triangle_p + \triangle_r = (m + 1/2)\lambda$,where m = 0,1,2...

Maxwell equations explain electromagnetic waves and describes how electromagnetic waves act in the material and vacuum. General Maxwell equations in the differential form are following,

Gauss's law : $\nabla \cdot \vec{E} = \frac{\rho}{\varepsilon_0}$

Gauss's law for magnetism: $\nabla \cdot \vec{B} = 0$

Faraday's law of induction : $\nabla \times \vec{E} = -\frac{\partial \vec{B}}{\partial t}$

Ampère-Maxwell law : $\nabla \times \vec{B} = \mu_0 \vec{J} + \mu_0 \varepsilon_0 \frac{\partial \vec{E}}{\partial t}$

In a vacuum ($\rho = 0, \mathbf{J} = 0$), Maxwell's equations will reduce to ;

Gauss's law : $\nabla \cdot \vec{E} = 0$

Gauss's law for magnetism: $\nabla \cdot \vec{B} = 0$

Faraday's law of induction : $\nabla \times \vec{E} = -\frac{\partial \vec{B}}{\partial t}$

Ampère-Maxwell law : $\nabla \times \vec{B} = \mu_0 \varepsilon_0 \frac{\partial \vec{E}}{\partial t}$

If we take curl of Faraday's law of induction and use Ampère-Maxwell law, we can get the magnetic and electric field ;

$$\vec{\nabla} \times (\vec{\nabla} \times \vec{E}) = \vec{\nabla} \times \left(-\frac{\partial \vec{B}}{\partial t} \right) \tag{2.5}$$

$$\vec{\nabla} \times \vec{\nabla} \times \vec{E} = \vec{\nabla}(\vec{\nabla} \cdot \vec{E}) - \nabla^2 \vec{E} = -\nabla^2 \vec{E} \tag{2.6}$$

$$\vec{\nabla} \times \left(-\frac{\partial \vec{B}}{\partial t} \right) = -\frac{\partial}{\partial t} \vec{\nabla} \times \vec{B} = -\frac{1}{c^2} \frac{\partial^2 \vec{E}}{\partial t^2} \tag{2.7}$$

$$\frac{\partial^2 \vec{E}}{\partial t^2} - c^2 \nabla^2 \vec{E} = 0 \tag{2.8}$$

When the equation 2.8 is solved and electric field equation is put into the Faraday's law of induction, magnetic field is obtained.

$$\vec{B} = \sqrt{\varepsilon_0 \mu_0} E_0 e^{i(\vec{k}\vec{r} - wt)} \tag{2.9}$$

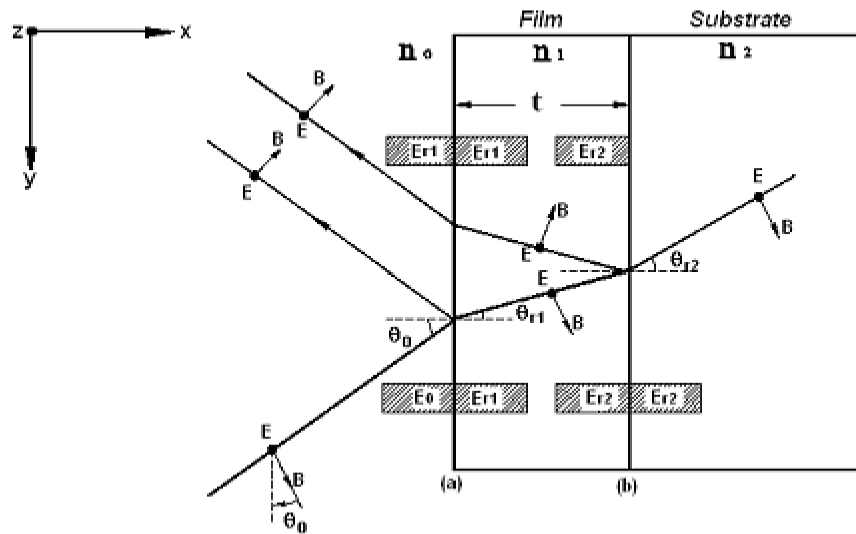

Figure 2.2: Reflection and refraction of a beam from a single layer .

After writing the magnitudes of electric field and magnetic field depending on the permittivity and permeability of medium they exist, we need to write electric field and magnetic fields at the boundary point.

Incident beam shown on the Figure 2.2 Electric field is perpendicular to the plane of incidence. There is an external reflection at the interface (a) which is separating the external medium of index n_0 from the film of index n_1. On the other hand, the beam undergoes internal

reflection at the plane interface (b) which is separating the thin film from substrate index n_s. The direction of E-field is -z along each beam, however, the direction of B-field is reversed on the reflection as it is shown on the Figure 2.2 .

If we apply boundary conditions, E_{r1} represents the sum of all reflected beams at the interface (a) and E_{i2} represents sum of all the multiple beams at the interface (b). Hence, we can calculate for the multiple beams in the interference according to the boundary conditions. The tangential components of E-field and B-field are continous at the interfaces, this means that the magnitude of the fields are equal on either side. E-field is tangential in every interface but B-field has both tangential component (y-direction) and perpendicular component (x-direction). As a result, the boundary conditions for the E-field are :

$$E_a = E_0 + E_{r1} = E_{t1} + E_{i1} \tag{2.10}$$

$$E_b = E_{i2} + E_{r2} = E_{t2} \tag{2.11}$$

On the other hand, the boundary conditions for the B-field are :

$$B_a = B_0 \cos\theta_0 - B_{r1} \cos\theta_0 = B_{t1} \cos\theta_{t1} - B_{i1} \cos\theta_{t1} \tag{2.12}$$

$$B_b = B_{i2} \cos\theta_{t1} - B_{r2} \cos\theta_{t1} = B_{t2} \cos\theta_{t2} \tag{2.13}$$

By using the equation 2.9 we can modify the equations 2.12 and 2.13,

$$B_a = \gamma_0(E_0 - E_{r1}) = \gamma_1(E_{t1} - E_{i1}) \tag{2.14}$$

$$B_b = \gamma_1(E_{i2} - E_{r2}) = \gamma_2 E_{t2} \tag{2.15}$$

where,

$$\gamma_0 \equiv n_0 \sqrt{\varepsilon_0\mu_0} \cos\theta_0 \tag{2.16}$$

$$\gamma_1 \equiv n_1 \sqrt{\varepsilon_0\mu_0} \cos\theta_{t1} \tag{2.17}$$

$$\gamma_s \equiv n_s \sqrt{\varepsilon_0\mu_0} \cos\theta_{t2} \tag{2.18}$$

Because of the phase difference there is a difference between E_{i2} and E_{t1} . Also there is a phase difference between the E_{i1} and E_{r2} .

$$E_{i1} = E_{r2}e^{-i\delta} \tag{2.19}$$
$$E_{i2} = E_{t1}e^{-i\delta} \tag{2.20}$$

The phase difference is stated as follows,

$$\delta = k_0\triangle = \left(\frac{2\pi}{\lambda_0}\right) n_1 t \cos\theta_{t1} \tag{2.21}$$

E_{i2} and E_{r2} which are stated in the boundary conditions (b) can be eliminated by using equation 2.19 and equation 2.20,

$$E_b = E_{t1}e^{-i\delta} + E_{i1}e^{i\delta} = E_{t2} \tag{2.22}$$
$$B_b = \gamma_1 E_{t1}e^{-i\delta} - E_{i1}e^{i\delta} = \gamma_s E_{t2} \tag{2.23}$$

If we solve the equations 2.22 and 2.23 for the E_{i1} and E_{t1} in terms of E_b and B_b we get;

$$E_{t1} = \left(\frac{\gamma_1 E_b + B_b}{2\gamma_1}\right) e^{i\delta} \tag{2.24}$$
$$E_{i1} = \left(\frac{\gamma_1 E_b - B_b}{2\gamma_1}\right) e^{-i\delta} \tag{2.25}$$

Then, substituting these equations into the equation 2.14 for the boundary point (a),

$$B_a = \left(\frac{\gamma_1 E_b + B_b}{2}\right) e^{i\delta} - \left(\frac{\gamma_1 E_b - B_b}{2}\right) e^{-i\delta} \tag{2.26}$$
$$= i\gamma_1 E_b \left(\frac{e^{i\delta} - e^{-i\delta}}{2i}\right) + B_b \left(\frac{e^{i\delta} + e^{-i\delta}}{2}\right)$$
$$B_a = i\gamma_1 E_b \sin\delta + B_b \cos\delta \tag{2.27}$$

In the same way, if we apply the same procedure for the E-field,

$$E_a = \left(\frac{\gamma_1 E_b + B_b}{2\gamma_1}\right) e^{i\delta} + \left(\frac{\gamma_1 E_b - B_b}{2\gamma_1}\right) e^{-i\delta} \quad (2.28)$$

$$E_a = E_b \cos\delta + B_b \left(\frac{i \sin\delta}{\gamma_1}\right) \quad (2.29)$$

Therefore, we can see that E-field and B-field at the boundary point (a) can be written in terms of E_b and B_b. These equations can be written also in matrix form as follows,

$$\begin{bmatrix} E_a \\ B_a \end{bmatrix} = \begin{bmatrix} \cos\delta & \left(\frac{i \sin\delta}{\gamma_1}\right) \\ \gamma_1 i \sin\delta & \cos\delta \end{bmatrix} \begin{bmatrix} E_b \\ B_b \end{bmatrix} \quad (2.30)$$

The (2 x 2) matrix is called transfer matrix of the thin film, shown as follows,

$$M = \begin{bmatrix} m_{11} & m_{12} \\ m_{21} & m_{22} \end{bmatrix} \quad (2.31)$$

If (b) is a boundary point of another thin layer instead of substrate, equation 2.30 is also valid. New characteristic matrix will be a form as follows,

$$\begin{bmatrix} E_a \\ B_a \end{bmatrix} = \underbrace{\mathbf{M}_1\mathbf{M}_2\mathbf{M}_3...\mathbf{M}_N}_{\mathrm{M_T}} \begin{bmatrix} E_b \\ B_b \end{bmatrix} \quad (2.32)$$

M_T is the overall transfer matrix and it shows multiplication of individual transfer matrices.

$\mathbf{M}_T = \mathbf{M}_1\mathbf{M}_2\mathbf{M}_3...\mathbf{M}_N$

Returning to the boundary conditions and putting them into the characteristic matrix, we can get the transmission and reflection of the thin film.

$$\left.\begin{aligned} E_a &= E_0 + E_{r1} \\ E_b &= E_{t1} \\ B_a &= \gamma_0(E_0 - E_{r1}) \\ B_b &= \gamma_s E_{t2} \end{aligned}\right\} = \begin{bmatrix} E_0 + E_{r1} \\ \gamma_0(E_0 - E_{r1}) \end{bmatrix} = \begin{bmatrix} m_{11} & m_{12} \\ m_{21} & m_{22} \end{bmatrix} \begin{bmatrix} E_{t2} \\ \gamma_s E_{t2} \end{bmatrix} \quad (2.33)$$

This matrix says us,

$$1 + r = m_{11}t + \gamma_s m_{12}\, t \tag{2.34}$$

$$\gamma_0(1 - r) = m_{21}t + \gamma_s m_{22}t \tag{2.35}$$

where, $t = \dfrac{E_{t2}}{E_0}$ and $r = \dfrac{E_{r1}}{E_0}$

When equations 2.34 and 2.35 are solved simultaneously transmission and reflection coefficient are found as,

$$t = \frac{2\gamma_0}{\gamma_0 m_{11} + \gamma_0\gamma_s m_{12} + m_{21} + \gamma_s m_{22}} \tag{2.36}$$

$$r = \frac{\gamma_0 m_{11} + \gamma_0\gamma_s m_{12} - m_{21} - \gamma_s m_{22}}{\gamma_0 m_{11} + \gamma_0\gamma_s m_{12} + m_{21} + \gamma_s m_{22}} \tag{2.37}$$

After finding the equations 2.36 and 2.37 transmission and reflection properties of a single layer or multilayer film can be evaluated.

Up to now,we have calculated all the equations depending on that E-field is perpendicular to the plane of incidence. When E-field is parallel to the plane of incidence, cosine factor in the expression for γ_1 will be in the denominator instead of in the numerator. Therefore,

For E-field $\perp$ plane of incidence : $\gamma_1 = n_1 \sqrt{\varepsilon_0\mu_0} \cos\theta_{t1}$

For E-field || plane of incidence : $\gamma_1 = n_1 \dfrac{\sqrt{\varepsilon_0\mu_0}}{\cos\theta_{t1}}$

For the normal incidence E-field is inseparable whether it is perpendicular or parallel to the plane of incidence because of $\cos\theta_{t1} = 1$. On the other hand, for oblique incidence transmission or reflection must be calculated in both parallel and perpendicular situation of E-field and then average must be taken for unpolarized light.

$$R = \frac{1}{2}(R_{\perp} + R_{||}) \tag{2.38}$$

$R_{\perp}$ is reflection for the E perpendicular to plane of incidence,

$R_{||}$ is reflection for the E parallel to plane of incidence.

2.2.1 Single Layer Antireflective (AR) Coating

When the incident beam strikes to the thin film at normal angle, $\cos\delta$ is equal to 1. In this case characteristic matrix becomes as ;

$$M = \begin{bmatrix} \cos\delta & \dfrac{i\sin\delta}{n_1\sqrt{\varepsilon_0\mu_0}} \\ in_1\sqrt{\varepsilon_0\mu_0}\sin\delta & \cos\delta \end{bmatrix} \tag{2.39}$$

If the elements of matrix is written in the equation 2.37 we get the equation,

$$\mathbf{r} = \frac{\gamma_0\cos\delta + \gamma_0\gamma_s\dfrac{i\sin\delta}{n_1\sqrt{\varepsilon_0\mu_0}} - in_1\sqrt{\varepsilon_0\mu_0}\sin\delta - \gamma_s\cos\delta}{\gamma_0\cos\delta + \gamma_0\gamma_s\dfrac{i\sin\delta}{n_1\sqrt{\varepsilon_0\mu_0}} + in_1\sqrt{\varepsilon_0\mu_0}\sin\delta + \gamma_s\cos\delta} \tag{2.40}$$

Substituting $\gamma_0, \gamma_1, \gamma_s$ into the equation 2.40 and then making cancellation and simplification, we obtain the equation,

$$r = \frac{n_1(n_0 - n_s)\cos\delta + i(n_0n_s - n_1^2)\sin\delta}{n_1(n_0 + n_s)\cos\delta + i(n_0n_s - n_1^2)\sin\delta} \tag{2.41}$$

The reflectance R is defined by, $R = \mid r^2 \mid$

r has a complex form as $r = \dfrac{A + iB}{C + iD}$

$$R = \mid r^2 \mid = \frac{A^2 + B^2}{C^2 + D^2} \tag{2.42}$$

Therefore,

$$R = \frac{n_1^2(n_0 - n_s)^2\cos^2\delta + (n_0n_s - n_1^2)^2\sin^2\delta}{n_1^2(n_0 + n_s)^2\cos^2\delta + (n_0n_s - n_1^2)^2\sin^2\delta} \tag{2.43}$$

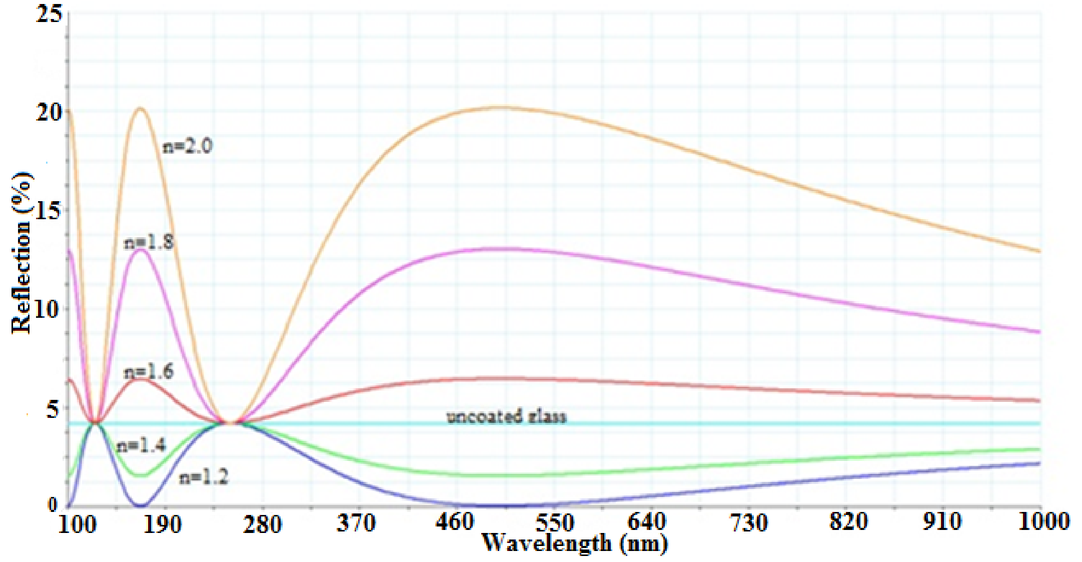

Figure 2.3: Reflection vs wavelength for single layer coatings designed with different refractive indices.

Figure 2.3 shows reflection versus wavelength for the different refractive indices. Uncoated glass has refractive index 1.52. The other curves represent single layer coating on the glass which has also refractive index 1.52. The parameter which determines that reflection for the coated glass is higher or lower than the uncoated glass is refractive index. If $n_1 > n_s$, reflection never can be lower than the uncoated glass reflection and if $n_1 < n_s$, reflection for the single layer coating can never higher than reflection for the uncoated glass at any wavelength. If the Figure 2.3 is examined carefully, we can see that reflection for the single layer coating is equal to the reflection for the uncoated glass at $\lambda/2$ wavelength. Phase difference which is depend on the optical path difference changes with the thin film thickness. At the film thickness $t = \lambda/4$,

$$\delta = \left(\frac{2\pi}{\lambda_0}\right) n_1 t \quad \xrightarrow{n=\lambda_0/\lambda} \quad \delta = \frac{\pi}{2} \tag{2.44}$$

Phase difference is equal to $\pi/2$ at odd multiples of quarter wavelength and it is equal to π at even multiples of quarter wavelength. If we look at reflection for this cases we obtain the equations 2.45 and 2.46 .

For the odd multiples of quarter wavelength,

$$t = (2m+1)\frac{\lambda}{4} \quad \Longrightarrow \quad R = \frac{(n_s n_0 - n_1^2)^2}{(n_s n_0 + n_1^2)^2} \tag{2.45}$$

For the even multiples of quarter wavelength,

$$t = (2m)\frac{\lambda}{4} \quad \Longrightarrow \quad R = \left(\frac{n_0 - n_s}{n_0 + n_s}\right)^2 \tag{2.46}$$

From these equations we can summarize that a perfect antireflective can be produced with quarter wavelength. When the numerator of the equation 2.45 is equated to zero,

$$n_1 = \sqrt{n_0 n_s} \tag{2.47}$$

If the substrate is chosen with $n = 1.52$, the most suitable refractive index is $n_1 = 1.23$, assuming $n_0 = 1$. In this case, magnesium fluoride is a logical option, with $n_1 = 1.38$.

2.2.2 Two Layer Antireflective (AR) Coating

Since coating materials that are available theoretically may not be found practically, so exact zero reflectance with single layer coating can not be possible. Because of this situation, double layer quarter wavelength coating is used for obtaining zero reflectance at a certain wavelength with available coating materials. At normal incidence,transfer matrix for the single layer quarter-wave coating is

$$M = \begin{bmatrix} 0 & \frac{i}{\gamma_1} \\ i\gamma_1 & 0 \end{bmatrix} \tag{2.48}$$

For the double layer coating, transfer matrix becomes

$$M = M_1 M_2 = \begin{bmatrix} 0 & \frac{i}{\gamma_1} \\ i\gamma_1 & 0 \end{bmatrix} \begin{bmatrix} 0 & \frac{i}{\gamma_2} \\ i\gamma_2 & 0 \end{bmatrix} = \begin{bmatrix} -\frac{\gamma_2}{\gamma_1} & 0 \\ 0 & \frac{-\gamma_1}{\gamma_2} \end{bmatrix} \tag{2.49}$$

If the elements of this matrix $m_{11} = \frac{\gamma_2}{\gamma_1}$, $m_{12} = 0$, $m_{21} = 0$, $m_{22} = \frac{\gamma_1}{\gamma_2}$ are put into the equation 2.37 reflection coefficient is found.

$$r = \frac{\gamma_2^2\gamma_0 - \gamma_s\gamma_1^2}{\gamma_2^2\gamma_0 + \gamma_s\gamma_1^2} \tag{2.50}$$

After finding the reflection coefficient, reflectance at normal incidence is calculated by using the equations 2.16 and 2.17 and 2.18,

$$R = \left(\frac{n_0 n_2^2 - n_s n_1^2}{n_0 n_2^2 + n_s n_1^2}\right) \tag{2.51}$$

Zero reflectance is found by equating the numerator of equation 2.51,

$$n_0(n_2)^2 = n_s(n_1)^2 \quad \longrightarrow \quad \frac{n_2}{n_1} = \sqrt{\frac{n_s}{n_0}} \tag{2.52}$$

For minimum reflection, this condition must be ensured. If refractive index is 1.52 for the glass and 1 for the incident air, ideal ratio (n_2/n_1) is 1.23 for the two coating materials. Zirconium dioxide ($n_2 = 2.1$) and cerium trifluoride ($n_1 = 1.65$) can be used to reach the ratio. The refractive index ratio of these two materials is 1.27 and this ratio produces 0.1 % according to the equation 2.51.

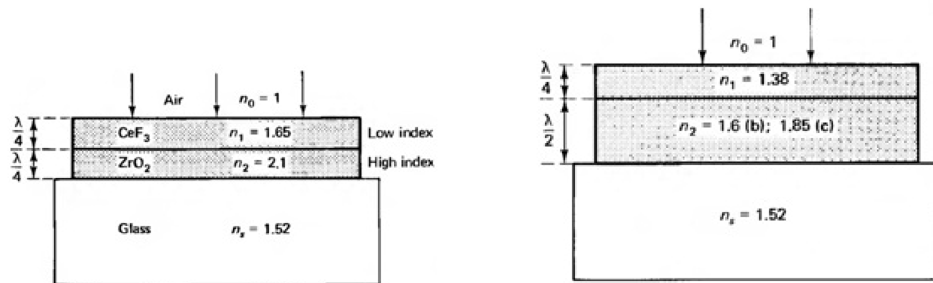

(a) Antireflecting double layer,using$\lambda/4 - \lambda/4$ thickness films.

(b) and (c) Antireflecting double layer,using$\lambda/4 - \lambda/2$ thickness films.

Figure 2.4: Antireflecting double layer using $\lambda/4 - \lambda/4$ and $\lambda/4 - \lambda/2$ thickness films [4].

Reflectance curves of (a), (b) and (c) are shown on the Figure 2.5 .

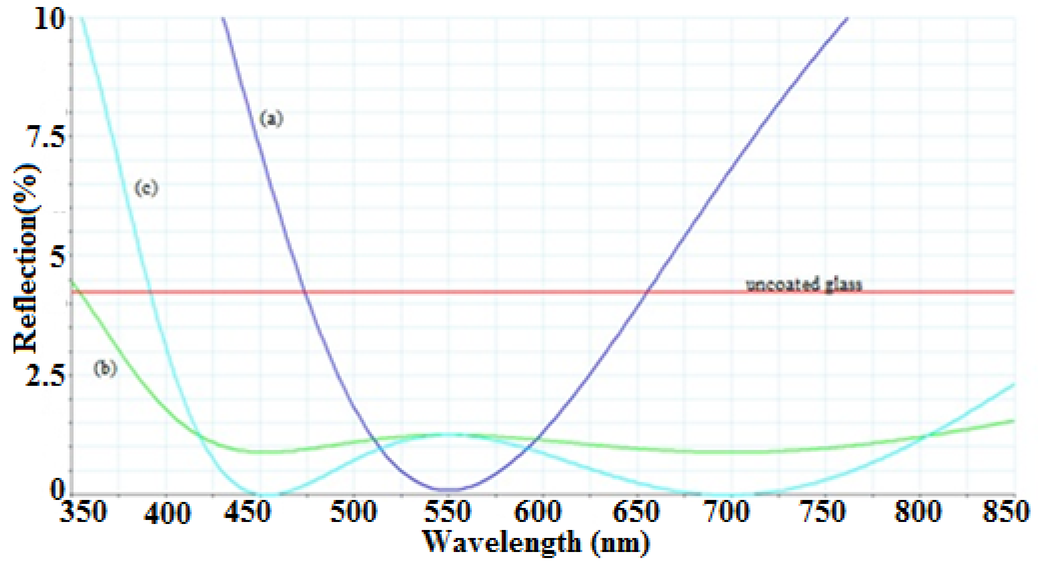

Figure 2.5: Reflectance vs Wavelength for the double layer coating. (a) quarter-quarter wavelength; $n_1 = 1.65, n_2 = 2.1$. (b) quarter-half wavelength; $n_1 = 1.38, n_2 = 1.6$. (c) quarter-half wavelength; $n_1 = 1.38, n_2 = 1.85$. $n_s = 1.52, n_0 = 1.0$ for all cases.

Figure 2.5 shows three different double layer antireflecting coatings. At the curve (a), reflectance goes to almost zero at 550 nm as it is not so low for the other wavelengths. Refractive index of the material which is adjacent to substrate should be lower than refractive index of substrate to get broadband antireflectance. This is available especially infrared region. For the visible region, restriction of $\lambda/4$ should be also changed to obtain broadband antireflective coatings . For instance, curves (b) and (c) represent $\lambda/4 - \lambda/2$ coatings. In this designs, thickness of a layer is changed as $\lambda/2$ so that broadband antireflectance is obtained.

2.2.3 Three Layer Antireflective (AR) Coating

Using three or more layer coatings can give a broader, lower and more flat reflectance region. When all of the layers are $\lambda/4$ thickness, nonreflective coating happens in the situation ;

$$\frac{n_1 n_3}{n_2} = \sqrt{n_0 n_s} \tag{2.53}$$

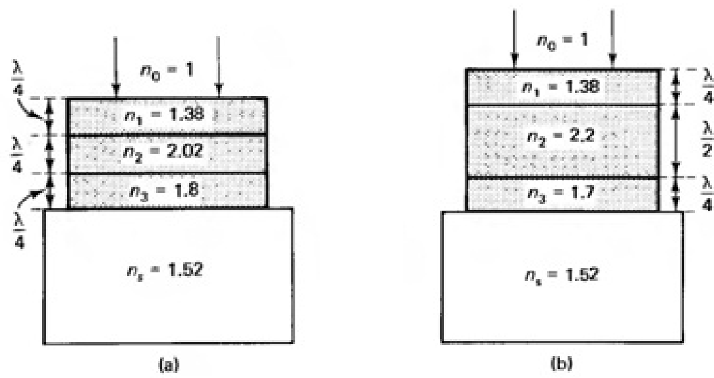

(a) Quarter-quarter-quarter wavelength layers.

(b) Quarter-half-quarter wavelength layers.

Figure 2.6: Antireflecting triple layers using $\lambda/4 - \lambda/4 - \lambda/4$ and $\lambda/4 - \lambda/2 - \lambda/4$ [4].

Reflecting curves of (a) and (b) are shown on the Figure 2.7 and some improvements are observed in the $\lambda/4 - \lambda/2 - \lambda/4$ wavelength layers as shown on the Figure 2.7.

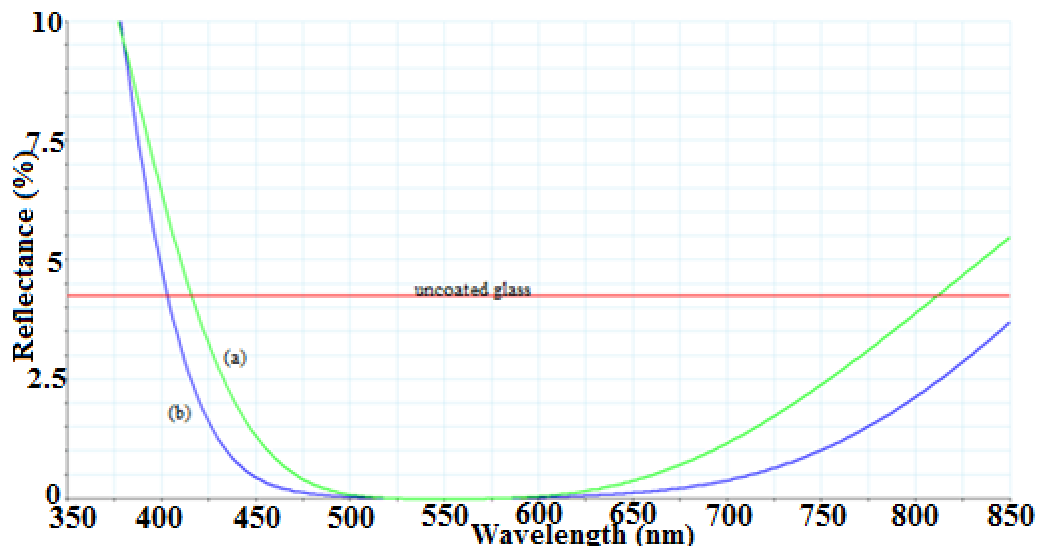

Figure 2.7: Reflectance vs wavelength for two different triple layer coating. (a) quarter-quarter-quarter wavelength ;$n_1 = 1.38$, $n_2 = 2.02$, $n_3 = 1.8$. (b)(b) quarter-half-quarter wavelength ; $n_1 = 1.38$, $n_2 = 2.2$, $n_3 = 1.7$. $n_0 = 1.0$, $n_s = 1.52$ and $\lambda = 550nm$ for two cases.

2.3 Reflective Coatings

2.3.1 Dielectric Mirrors

When the layer order of a double layer antireflective coating is reversed, namely, the order is air-high index-low index- substrate, reflected lights will be in same phase and reflection will be increased. A series of the such double layers raises the reflectance and this structure is called a dielectric mirror [4].

If we write the transfer matrix for the double layer quarter wavelength thickness,

$$M_{HL} = M_H M_L = \begin{bmatrix} 0 & \dfrac{i}{\gamma_H} \\ i\gamma_H & 0 \end{bmatrix} \begin{bmatrix} 0 & \dfrac{i}{\gamma_L} \\ i\gamma_L & 0 \end{bmatrix} = \begin{bmatrix} -\dfrac{\gamma_L}{\gamma_H} & 0 \\ 0 & -\dfrac{\gamma_H}{\gamma_L} \end{bmatrix} \tag{2.54}$$

where,

M_H : Characteristic matrix for high refractive index,

M_L : Characteristic matrix for low refractive index,

and for the series of double layers,

$$M_{HL} = (M_{H1}M_{L1})(M_{H2}M_{L2})(M_{H3}M_{L3})...(M_{HN}M_{LN}) = (M_{HL})^N \tag{2.55}$$

$$M_{HL} = \begin{bmatrix} -\dfrac{\gamma_L}{\gamma_H} & 0 \\ 0 & -\dfrac{\gamma_H}{\gamma_L} \end{bmatrix}^N = \begin{bmatrix} \left(-\dfrac{\gamma_L}{\gamma_H}\right)^N & 0 \\ 0 & \left(-\dfrac{\gamma_H}{\gamma_L}\right)^N \end{bmatrix} \tag{2.56}$$

For the normal incidence,

$$\frac{\gamma_L}{\gamma_H} = \frac{n_L}{n_H} \tag{2.57}$$

therefore,

$$\mathbf{M} = \begin{bmatrix} \left(-\dfrac{n_L}{n_H}\right)^N & 0 \\ 0 & \left(-\dfrac{n_H}{n_L}\right)^N \end{bmatrix} \tag{2.58}$$

If the reflection coefficient is solved by using the matrix elements, reflection coefficient will be,

$$\boldsymbol{r} = \frac{n_0(-n_L/n_H)^N - n_s(-n_H/n_L)^N}{n_0(-n_L/n_H)^N - n_s(-n_H/n_L)^N} \tag{2.59}$$

and by editing the reflection coefficient, reflectance is obtained as follows,

$$\boldsymbol{R} = \left(\frac{(n_0/n_s)(n_L/n_H)^{2N} - 1}{(n_0/n_s)(n_L/n_H)^{2N} + 1}\right)^2 \tag{2.60}$$

For the different N numbers, three different dielectric mirror designs are shown on the Figure 2.8.

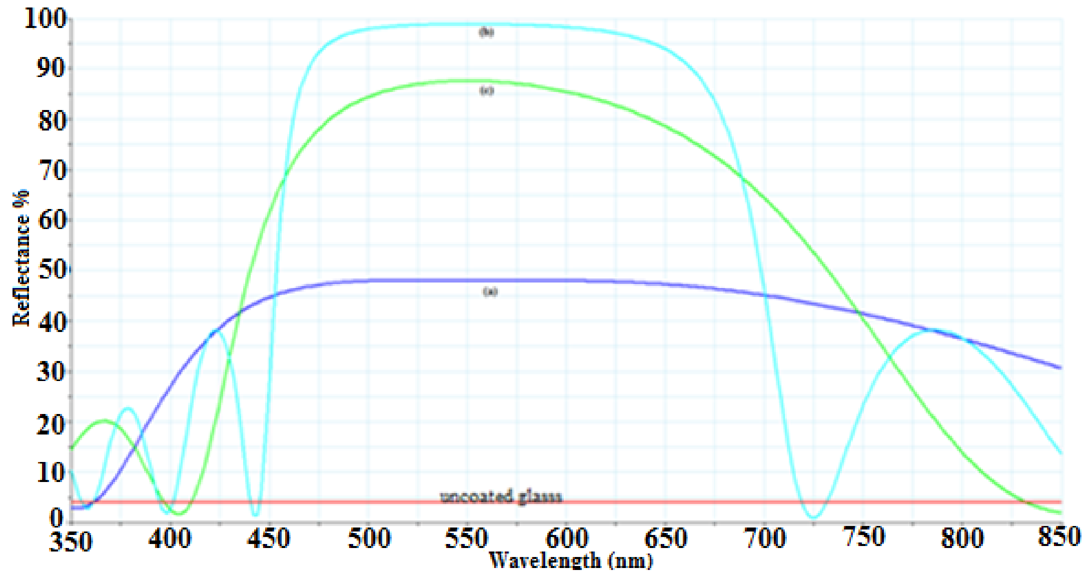

Figure 2.8: Reflectance vs Wavelength for three different dielectric mirrors.(a) $N = 2$ double layers. (b) $N = 6$ double layers.(c) $N = 2$ double layers with an additional high index layer. $n_0 = 1.0$, $n_s = 1.52$, $n_H = 2.35$, $n_L = 1.38$ and layers are quarter wavelength at $\lambda = 550$ nm.

2.3.2 High Reflective Metallic Coatings

Apart from the dielectric mirrors, there is an another method which is called high reflective metallic coatings for the reflective coatings. Aluminum (Al), Silver (Ag) and Gold (Au) are the most common materials for the high reflective coatings. Because of its cheapness, Al is the most commonly used material for high reflective coatings and the purpose of the using these materials changes through the spectrum. For instance, Ag is a very suitable material through the far infrared spectrum. On the other hand, Au is a perfect material for the infrared region but it is an expensive material and it is not so suitable material through the visible spectrum. Reflectance vs Wavelength is shown on the Figure 2.9 for these and some other materials.

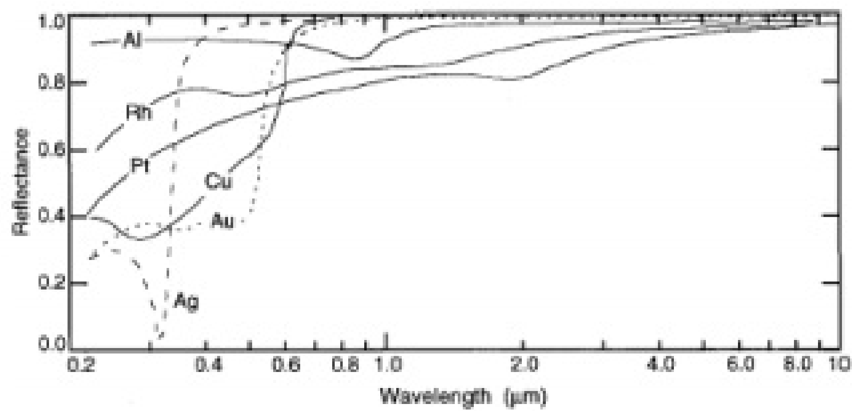

Figure 2.9: Reflectance vs Wavelength for some materials [5].

Since metallic coatings are weak against chemical and mechanical damages, they should be protected with protective layers. These protective layers are designed as antirefleective coating. In such a coating dielectric material that has a low refractive index is coated on the metallic surface. For example, Silicon dioxide, Silicon oxide and Magnesium fluoride can be used as a protective material on the Aluminum and Aluminum oxide is the material for protecting silver surface [6].

For the metallic materials refractive index is that ;

$$N = n - i\kappa \tag{2.61}$$

n is the real part of the refractive index, κ is the extinction coefficient

Reflection coefficient is $r = \dfrac{E_{r1}}{E_0}$ and reflectance is $R = rr^*$

If reflectance is solved with respect to above equations for the normal incidence,

$$R = \frac{(n-1)^2 + \kappa^2}{(n+1)^2 + \kappa^2} \tag{2.62}$$

is obtained as the reflectance.

When we calculate reflectance of some materials for the normal incidence we obtain a table like table 2.10 .

Table 2.1: Reflectance of Aluminum, Silver and Gold [7].

λ(μm)	R (%)		
	Al	Ag	Au
	91.5		
0.220	91.9	28.0	27.5
0.240	92.2	29.5	31.6
0.260	92.3	29.2	35.6
0.280	92.3	25.2	37.8
0.300	92.4	17.6	37.7
0.315	92.4	5.5	37.3
0.320	92.5	8.9	37.1
0.340	92.5	72.9	36.1
0.360	92.5	88.2	36.3
0.380	92.4	92.8	37.8
0.400	92.2	95.6	38.7
0.450	91.8	97.1	38.7
0.500	91.5	97.9	47.7
0.550	91.1	98.3	81.7
0.600	90.5	98.6	91.9
0.650	89.7	98.8	95.5
0.700	88.6	98.9	97.0
0.750	86.7	99.1	97.4
0.800	86.7	99.2	98.0
0.850	89.1	99.2	98.2
0.900	92.4	99.3	98.4
0.950	94.0	99.3	98.5
1.0	97.4	99.4	98.6
1.5	97.8	99.4	99.0
2.0	98.0	99.4	99.1
3.0	98.2	99.4	99.3
4.0	98.4	99.4	99.4
5.0	98.5	99.5	99.4
6.0	98.6	99.5	99.4
7.0	98.7	99.5	99.4
8.0	98.7	99.5	99.4
9.0	98.7	99.5	99.4
10.0	98.9	99.5	99.4
15.0	99.0	99.6	99.4
20.0	99.2	99.6	99.4
30.0	99.2	99.6	99.4

CHAPTER 3

THIN FILM DEPOSITION TECHNIQUES

3.1 Introduction

In this chapter, how thin film deposition is done will be discussed and also different methods of thin film production will be explained. Moreover , these methods will be compared with each other.

3.2 Thin Film Deposition Methods

There are some methods for the production of thin films. Most of these methods are under vacuum and they can be classified as physical vapour deposition (PVD). In these processes, the thin film condenses directly in the solid phase from the vapour [3]. Mechanical or electromechanical forces are used in physical vapour deposition. Typically, PVD processes are used to deposit films with thicknesses in the range of a few nanometers to thousands of nanometers; however they can also be used to form multilayer coatings, graded composition deposits, very thick deposits and freestanding structures [2].

Chemical vapour deposition (CVD) technique is another method for the production of thin films. A fluid precursor is used in CVD and it leads to a chemical change at a solid surface.

Main difference between physical and chemical deposition techniques is related to how the atoms that are comprised the film are directed to the substrate. Since the thin film material is exposed to a fluid, chemical deposition is conformal. Therefore, chemical deposition approaches to the substrate without a particular direction. On the other hand, in physical depo-

sition techniques that depends on mechanical or electromechanical forces , particles deposited are brought to the substrate by using temperature or pressure parameters. Hence , in the physical thin film deposition techniques, atoms or molecules that are deposited are directed from the target to the substrate.

3.2.1 Chemical Vapor Deposition (CVD)

Source material is in the gases form in the chemical vapour deposition method. In this method, fluid precursor is formed by depositing coating material and this is in the gases form. Decomposition is performed by thermal activation. The deposited material may react with other gaseous species in the system to give compounds (e.g. oxides, nitrides) [2]. Gas absorption is done by the substrate surface.Coating process occurs between the precursor and substrate chemically until reaching the required thickness.

CVD is classified according to some parameters like phase of coating material , plasma supported or not.

As single crystal films is used for deposition, chemical vapour deposition is called Vapor Phase Epitaxy (VPE). Another type of CVD is Metalorganic CVD (MOCVD). When Metalorganic species are used as the precursor gas , that is called Metalorganic CVD. The other type of CVD is Plasma Enhanced CVD (PECVD) . Plasma is used in this method to activate decomposition and reaction and when the pressure is less than ambient ,this type of CVD is called Low Pressure CVD (LPCVD) [2] .

3.2.2 Physical Vapor Deposition (PVD)

The other main thin film production technique is physical vapour deposition (PVD). PVD is the process which is depositing a material in the solid or liquid phase to the substrate where it condenses through the very low pressure.The thickness of the coated material can be in the range of several nanometers to microns. Different from the CVD , coating material is in the solid or liquid phase. Some techniques of the PVD are going to be explained.

3.2.2.1 Thermal Evaporation

Thermal evaporation is the basic and simplest one in the evaporation and physical vapour deposition methods. In this method , coating material is heated and evaporated by the resistance that is generally filament and the evaporated material is condensed on the substrate. This process is made under high vacuum . The purposes of doing process under vacuum are preventing unwanted oxidization of the boiling material and reducing the impurity of deposition [8]. This method is used generally for the reflective coating and silver , Gold and Aluminum are the most used materials for coating. Because of using very high voltage to evaporate coating material the crucible where the coating material is put in should have high melting temperature. So, Tungsten (W) , Tantalum (Ta) and Molybdenum (Mo) are very common materials for the crucible. Mildness is an advantage of the thermal evaporation but there is a contamination problem in this method. Crucible material can also evaporate , so this situation may lead to contamination of deposited film. The another problem of this method is the inability of the deposit refractory material, like oxide compounds .

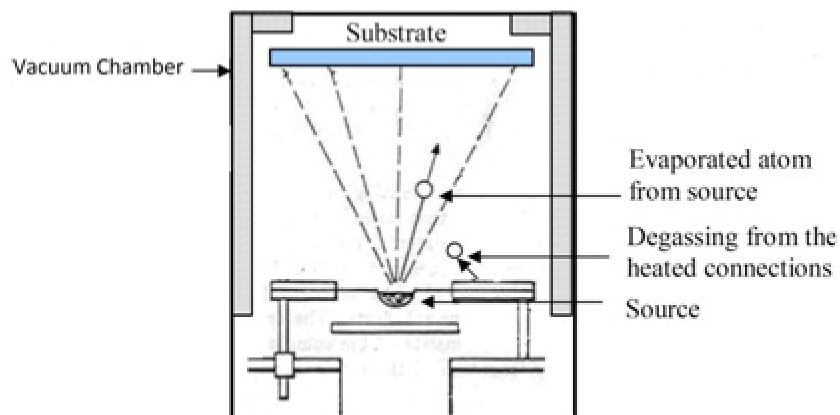

Figure 3.1: Thermal Evaporation in a coating system

3.2.2.2 Electron Beam Evaporation

The other evaporation technique is electron beam evaporation. Not only metals but also dielectric materials can be used as coating materials with electron beam evaporation method. In this method coating material is heated directly, not heated by a crucible. A filament is used for emitting the electrons. AC current is given to the filament to get the electrons and then emitted electrons are directed to the target with the influence of the magnetic field. In this way,

high temperature can be obtained more effectively. Recently , this method has been a very common process because of some advantages. One of the advantages is that the crucibles are cooled with water so that crucibles can not be evaporated and coating that has low impurity can be obtained. The other advantage of this method is that different coating materials can be evaporated sequentially by using more than one crucible. In this way, multilayer coating can be done in one process. On the other hand, there are disadvantages for this method. The main disadvantage of them is difficulty of getting high packing density since deposited atoms have low energy or mobility [8].

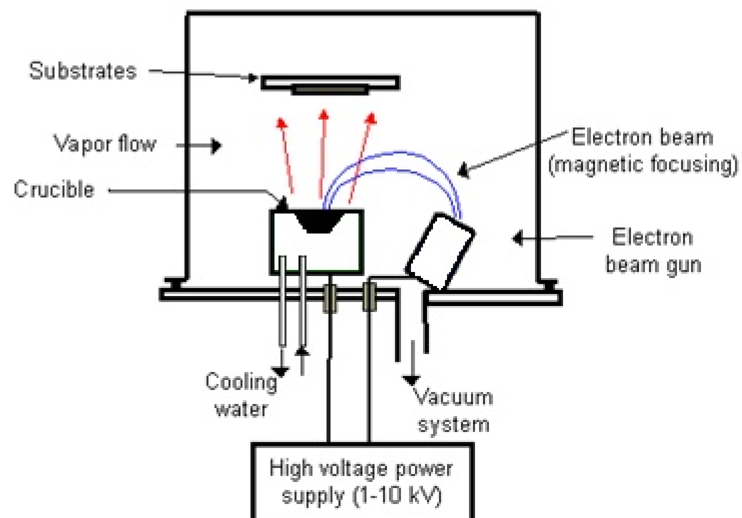

Figure 3.2: Electron Beam evaporation system

Furthermore, there could be a huge difference between the minimum points of evaporation temperature for some materials and the Table 3.1 shows the minimum point of evaporation temperature for the coating materials . Also, crucible materials are recommended for most of the coating materials with deposition rate and power.

Table 3.1: Evaporation Characteristics of coating Materials [9].

Material	**Minimum[a] Evap. Temp.**	**State of Evaporation**	**Recommended Crucible Material**	**e-beam[b]** Deposition Rate(A/s)	Power (kW)
Aluminum	1010	Melts	BN	20	5
Aluminum oxide	1325	Semimelts		10	0.5
Antimony	425	Melts	BN, Al_2O_3	50	0.5
Arsenic	210	Sublimes	Al_2O_3	100	0.1
Berylum	1000	Melts	Graphite, BeO	100	1.5
Berylum oxide		Melts		40	1.0
Boron	1800	Melts	Graphite, WC	10	1.5
Boron carbide		Semimelts		35	1.0
Cadmium	180	Melts	Al_2O_3 ,Quartz	30	0.3
Cadmium sulfide	250	Sublimes	Graphite	10	0.25
Calcium fluoride		Semimelts		30	0.05
Carbon	2140	Sublimes		30	1.0
Chromium	1157	Sublimes	W	15	0.3
Cobalt	1200	Melts	Al_2O_3, BeO	20	2.0
Copper	1017	Melts	Graphite,Al_2O_3	50	0.2
Gallium	907	Melts	Al_2O_3,Graphite		3.0
Germanium	1167	Melts	Graphite	25	3.0
Gold	1132	Melts	Al_2O_3 ,BN	30	6.0
Indium	742	Melts	Al_2O_3	100	0.1
Iron	1180	Melts	Al_2O_3 .BeO	50	2.5
Lead	497	Melts	Al_2O_3	30	0.1
Lithium fluoride	1180	Melts	Mo, W	10	0.15
Magnesium	327	Sublimes	Graphite	100	0.04
Magnesium fluoride	1540	Semimelts	Al_2O_3	30	0.01
Molybdenum	2117	Melts		40	4.0
Nickel	1262	Melts	Al_2O_3	25	2.0
Permalloy	1300	Melts	Al_2O_3	30	2.0
Platinum	1747	Melts	Graphite	20	4.0
Silicon	1337	Melts	BeO	15	0.15
Silicon dioxide	850	Semimelts	Ta	20	0.7
Silicon monoxide	600	Sublimes	Ta	20	0.1
Tantalum	2590	Semimelts		100	5.0
Tin	997	Melts		10	2.0
Titanium	1453	Melts		20	1.5
Titanium dioxide	1300	Melts	W	10	1.0
Tungsten	2757	Melts		20	5.5
Zinc	250	Sublimes		50	0.25
Zinc selenide	660	Sublimes	Quartz		
Zinc sulfide	300	Sublimes	Mo		
Zirconium	1987	Melts	W	20	5.0

[a] : Temperature ° C at which vapor pressure is 10^{-3} torr.

[b] : For 10 kV , copper hearth , source-substrate distance of 40 cm.

3.2.2.3 Sputtering

Sputtering which is also called sputter deposition is a deposition process of vaporized atoms or molecules from target material. In this method, surface atoms of target are emitted by momentum transfer from an atomic-sized energetic bombarding particle that is generally a gaseous ion accelerated from plasma and this is non-thermal vaporization process [2]. The ions that have high kinetic energy can be also from a solid surface in a vacuum. Sputter deposition can be either in a low pressure plasma or in a higher plasma pressure. In the low pressure plasma that is lower than 5 mTorr, sputtered particles suffer few or no gas phase collisions in the space between the target and the substrate. On the other hand, in the high pressure plasma that is between 5-30 mTorr sputtered particles are thermalized by gas phase collisions before arriving to the substrate surface [2] . There are mainly three types of sputter deposition which are Ion Beam sputtering, Magnetron Sputtering and RF Sputtering. By using especially Ion Beam Sputtering method, coating that have dense layers without scattering and absorption can be obtained and this method eliminates spectral shift [10]. Another advantage of the sputter deposition especially for the magnetron sputtering is that coating process that has high deposition rate , low deposition pressure and low substrate temperature can be obtained [10].

Table 3.2: Comparison between Evaporation and Sputtering methods [11].

Evaporation	**Sputtering**
Low energy atoms ($\sim 0.1eV$)	High Energy atoms / ions $(1-10eV)$ - denser film - smaller grain size - better adhesion
High Vacuum - directional , good for lift-off - lower impurity	Low Vacuum - poor directionality , better step coverage - gas atom implanted in the film
Point Source - poor uniformity	Parallel Plate Source - better uniformity
Component Evaporate at Different Rate - poor stoichiometry	All Component Sputtered with Similar Rate - maintain stoichiometry

3.2.2.4 Ion Assisted Deposition (IAD) and Plasma Ion Assisted Deposition (PIAD)

Ion assisted deposition method which is also called Ion plating is a transferring process of depositing material that is evaporized either by evaporation, sputtering or by decomposition of a chemical vapor precursor to the substrate with the help of bombardment of energetic particles. In ion assisted deposition ,generally, ions of an inert or reactive gas ,or, in some case ions of the condensing film material are used as the energetic particles [2] . The most important property of this method is that coatings which have a higher refractive index than would be obtainable by evaporation method can be obtained. Another advantage of this method is providing a high adhesion force between substrate and coated material. Moreover, this method is used to deposit hard coatings of compound materials, adherent metal coatings and conformal coatings on complex surfaces [2]. A general setup of Ion beam assisted deposition method is shown on the Figure 3.3.

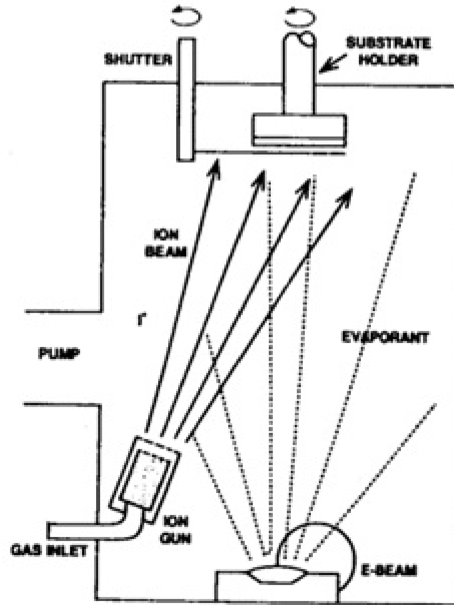

Figure 3.3: Ion Beam Assisted deposition [2].

On the other hand, plasma can be used with Ion assisted deposition and this method is called Plasma ion assisted deposition (PIAD). This method is applied usually at low temperature. Using plasma with ion assisted deposition has some advantages. PIAD is faster than sputtering and complex compositions can be done with this technique [12]. Coatings which are done with PIAD method minimizes wavelength shift and it has also good adhesion. PIAD method is used for not only dielectric coatings but also metal coatings. As a result, Plasma ion assisted deposition can notably enhance the performance of antireflection coatings, narrow-wide pass band filters, edge filters, abrasion-resistant transparent films, dielectric mirrors, Rugate filters and gain-flattening filters [10]. A general setup of a PIAD method is shown on the Figure 3.4.

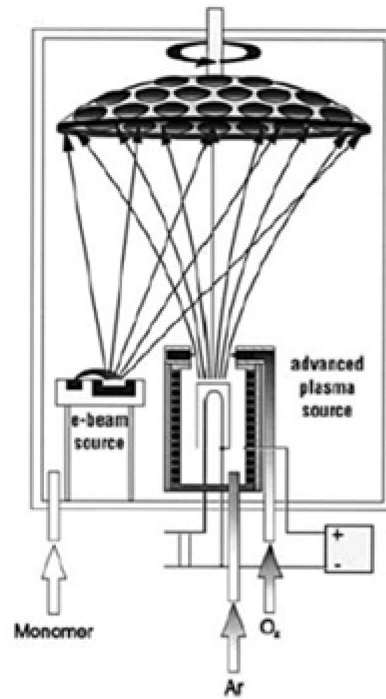

Figure 3.4: Setup of a Plasma Ion-Assisted Deposition [13].

If we look at chemical and physical vapor deposition techniques and make a comparison, we can make a table like Table 3.3.

Table 3.3: Camparison of Typical Thin Film Deposition Techniques [11].

Process	Material	Uniformity	Impurity	Grain Size	Film Density	Deposition Rate	Substrate Temperature	Directional
Themal Evaporation	Metal or low melting point materials	Poor	High	10-100 nm	Poor	1-20 A/s	50-100 °C	Yes
E-beam Evaporation	Both metal and dielectrics	Poor	Low	10-100 nm	Poor	10-100 A/s	50-100 °C	Yes
Sputtering	Both metal and dielectrics	Very good	Low	~10 nm	Good	Metal : ~100 A/s Dielectric: 1-10 A/s	~200 °C	Some degree
PECVD	Mainly dielectrics	Good	Very low	10-100 nm	Good	10-100 A/s	200-300 °C	Some degree
LPCVD	Mainly dielectrics	Very good	Very low	1-10 nm	Excellent	10-100 A/s	600-1200 °C	Isotropic

3.3 Optical Coating System

Optical coating system that was used for the production of designed filters is shown on the Figure 3.5. It can reach high vacuum about 10^{-6} - 10^{-7} mbar pressure and it can make a multilayer process without a break . Components of the system that are thermal evaporation unit, electron beam unit evaporation, advanced plasma source and thickness measuring units are going to be explained briefly .

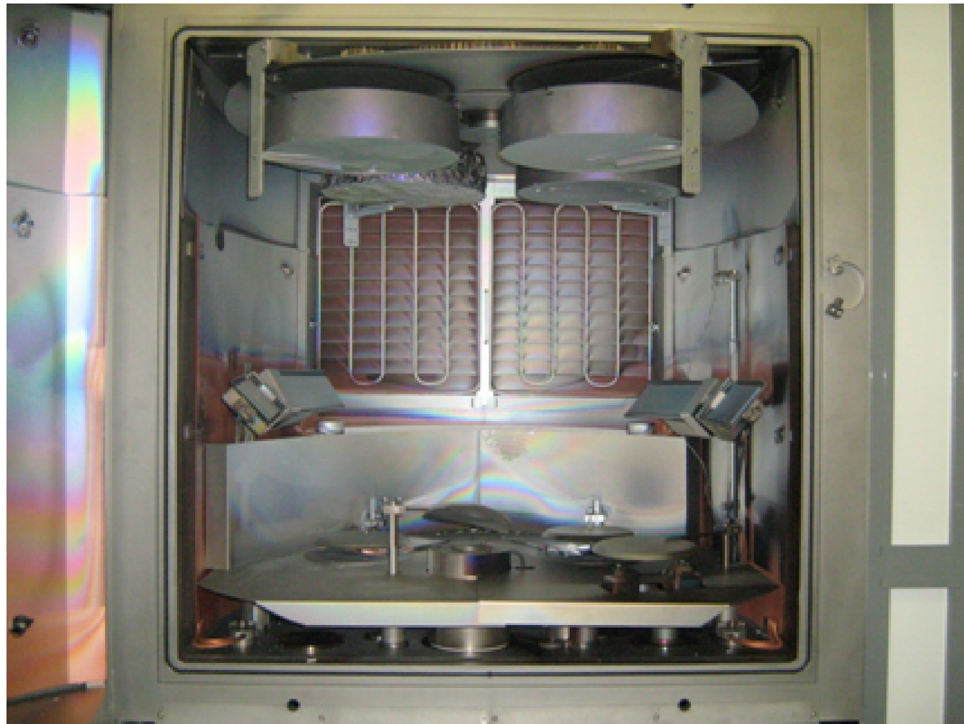

Figure 3.5: Optical Coating System

3.3.1 Evaporation Units

There are two types of evaporation units inside the system :

- Electron beam evaporation
- Thermal evaporation

With these units, both of the metal and dielectric coatings can be made easily. Electron beam evaporator is used usually for the dielectric materials and thermal evaporator is used

generally for the metal coatings. Pictures of the electron beam evaporation units are shown on the Figure 3.6 and Figure 3.7. Thermal evaporation unit is shown on the Figure 3.8.

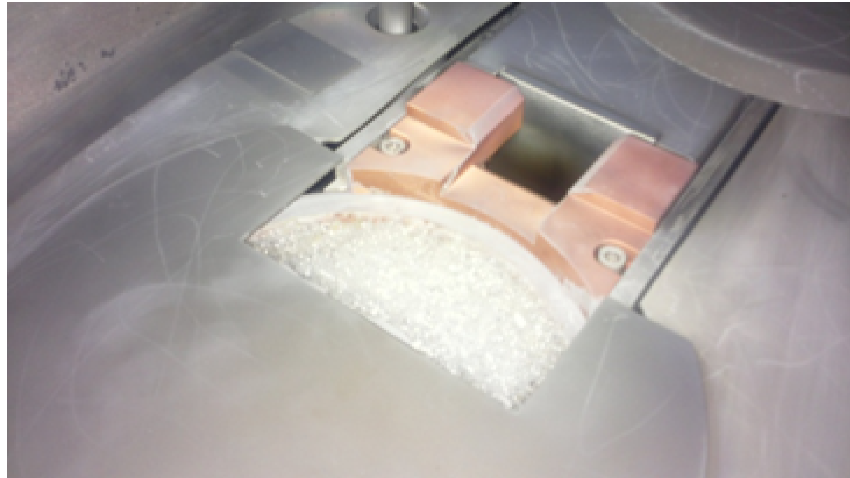

Figure 3.6: Electron beam evaporation unit 1

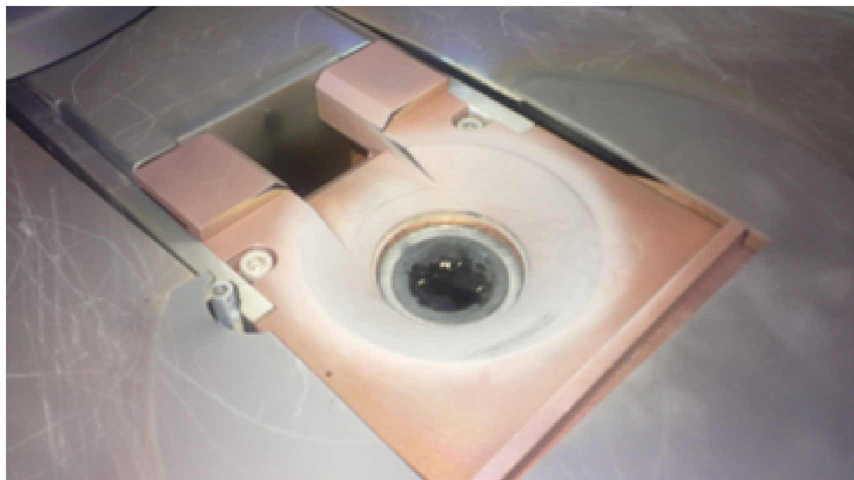

Figure 3.7: Electron beam evaporation unit 2

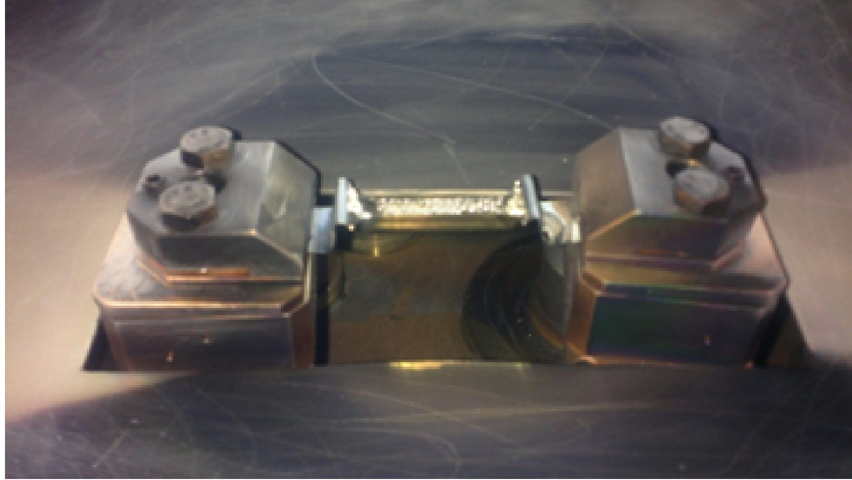

Figure 3.8: Thermal evaporation unit

3.3.2 Advanced Plasma Source

Advanced plasma source provides a plasma into the vacuum chamber in order to make qualified coating. Plasma supported coating process has the following main advantages :

- Increased density, adhesion, hardness and scratch resistance of the coating,
- Lower operating temperatures and thus better conditions for coating heat-sensitive substrates,
- High deposition rates and thus shorter process time,
- Temperature-stable coatings over large surfaces,
- Flat boundary layers and amorphous layer structures that lead to very low dispersion or absorption losses.[14]

Plasma source is composed of LaB_6 cathode , graphite heater and anode tube. Plasma is formed by electrons that are broken from cathode and gas sources which are Argon and Oxygen. Graphite heater is heated up to the 1500 $°C$ to obtain the electrons. Electrons are directed and accelarated by the DC voltage between the anode and cathode. Accelarated electrons create the plasma by colliding with the gas atoms. Structure of the Advanced plasma source is shown on the Figure 3.9 and APS parameters that are used in the production are shown on the Table 3.4.

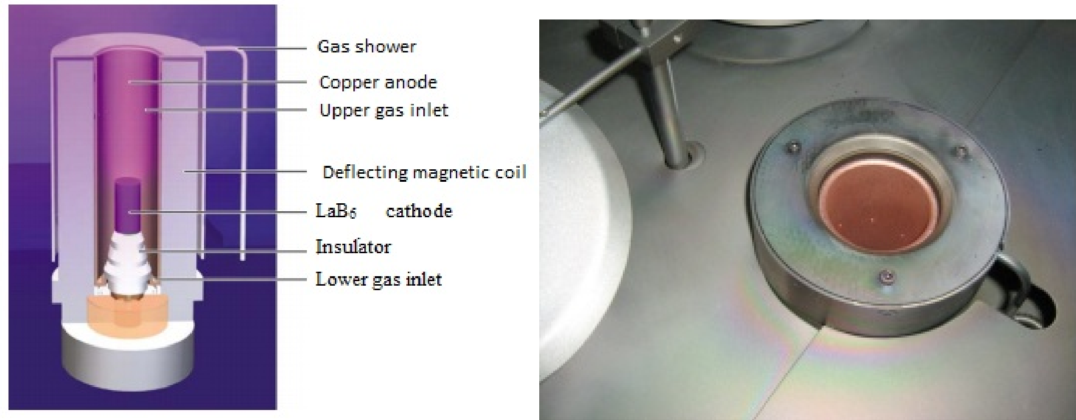

Figure 3.9: Advanced plasma source [14].

Table 3.4: APS Parameters

Material	Etch	PreCon APS	SiO2	Ti3O5/ Ti2O3	Ta2O5	Al2O3	SiO	MgF2	ITO
Rate	-	-	0.5-1.0	0.25-0.35	0.2-0.5	0.3	0.2	0.5-1.2	0.25
Z-Ratio	-	-	1	1	0.3	0.336			1.0
Density	-	-	2.64	4.26	8.20	3.97			8.17
Coil Current [A]	1.20	1.20	1.50	1.50	1.50	1.6	-	-	-
Temperature [C°]	-	-	-	-	-	-	-	250-350	-
Discharge Current [A]	40-50	50-60	50-60	40-50	40-50	50	-	-	60
Bias Voltage [V]	80-100	0.0	130-180	100-110	100-130	130-140	-	-	80.0
Ar #1 Flow [sccm]	8-12	12.0	2.0-3.0	4-6	4-6	5-8	-	-	7
Ar #2 Flow [sccm]	0-5	0.0	12.0-16.0	5-9	5-9	0-7	-	-	10
O2 Flow [sccm]	0-5	0	3-20	22-35	20-35	15-30			10

3.3.3 Thickness Measurement Unit

There are two types coating thickness measuring devices in the system that is used for designed filters. These are Quartz crystal measuring unit and Optical layer thickness measuring unit (OMS).

To determine the coating thickness and deposition rate, changing oscillation frequency of a simultaneously coated quartz crystal is measured in the quartz crystal measuring system. When the mass of coating material increases , oscillation frequency decreases. In the quartz crystal measuring system , quartz crystal oscillates at high frequency which is approximately 6 MHz [14] .

The other optical thickness measuring device is Optical layer thickness measuring unit (OMS). In the OMS, thickness of the coated material is determined by transmission or reflection of the coating that is measured by dual-beam photometer inside the unit. OMS includes optomechanical components like the chopper, monochromator, light source, detector and the control system. Switch off of the layer thickness is controlled by the sophisticated monitoring software [14] .

The components of the OMS are shown on the Figure 3.10 and the picture of OMS test glass and Quartz Crystal inside the system is shown on the Figure 3.11.

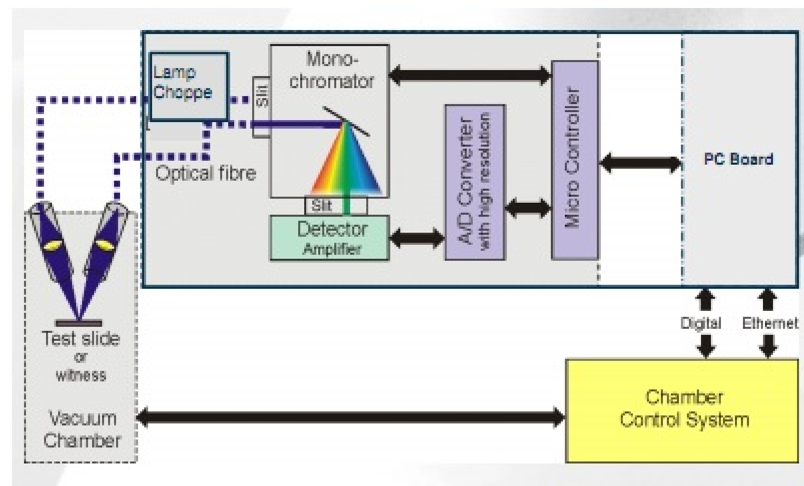

Figure 3.10: Optical Monitoring System [14].

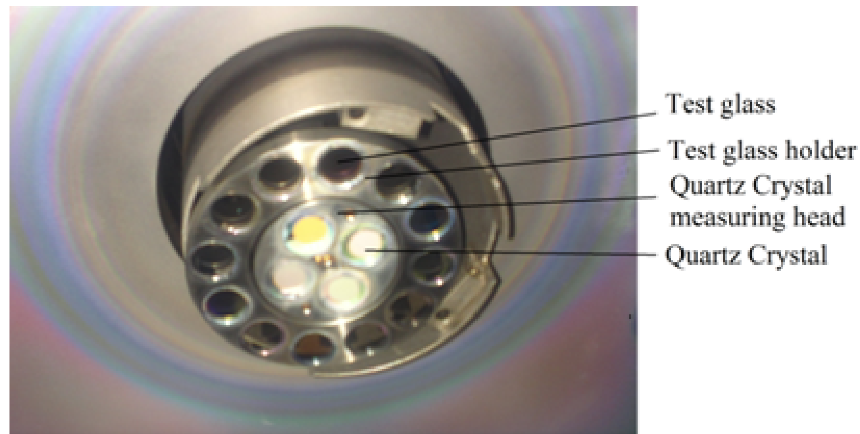

Figure 3.11: OMS and Quartz Crystal measuring unit.

3.3.4 Characterization

Characterization of the produced filters was done by using a spectrophotometer. The spectrophotometer can make measurement in the UV, visible and NIR spectral region by using pre-aligned tungsten, halogen and deuterium lamp. Transmission and reflection can be measured in the wavelength range of 175nm-3300nm through the three detector module in the spectrophotometer. The detector module has a PMT detector for the UV/Vis range and a InGaAs detector and PbS for the near infrared spectrum region. The spectrophotometer that was used to measure the transmission and reflection spectrum is shown on the Figure 3.12 and some specifications of the spectrophotometer are shown on the Table 3.5.

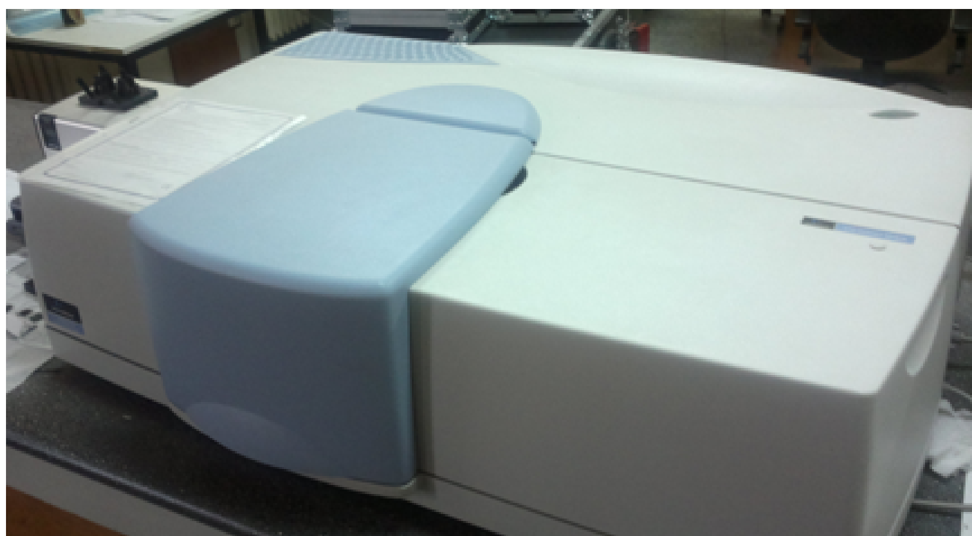

Figure 3.12: Spectrophotometer

Table 3.5: Spectrophotometer specifications

Specification	**Perkin Elmer Lambda 950**
Detectors	Combination of Peltier-cooled, Narrowband InGaAs detector covering 860-1800 nm and PbS detector covering 1800-3300 nm in the NIR wavelength range
Source	Pre-aligned tungsten-halogen and deuterium lamps.
Wavelength Range	175-3300 nm
UV/Vis Resolution	≤0.05 nm
NIR Resolution	≤0.20 nm
Wavelength Accuracy	± 0.080 nm UV/Vis ± 0.30 nm NIR
Instrument Requirements Power Temperature Recommended Humidity	 90 VAC-250 VAC, 50/60 Hz;250 VA 10-35 °C 10%-70% relative humidity, non-condensing.

CHAPTER 4

DESIGN AND PRODUCTION OF NEAR INFRARED INTERFERENCE FILTER

4.1 Introduction

Before production of a Near Infrared Interference filter, designs and suitable materials have been studied on. Since SiO_2, TiO_2 and MgF_2 are commonly used materials for the visible and near infrared spectral region, these materials have been chosen in the designs. Designs of the Near Infrared Interference filter that block the visible (400nm-700nm) spectral region and transmits the near infrared (700nm-1400nm) spectral region have been worked on awhile. The number of layers in the design have been tried to minimize to ease production. When we have used MgF_2 as a low refractive index material in the design we have obtained very good transmission and reflection spectrums. However, when we produced the filters, transmission and reflection measurements were not so good. Since chemical bonds between the TiO_2 and MgF_2 are not very good we decided that MgF_2 was not a suitable material with oxide dielectric materials. Finally, we have decided to use designs that consist of $SiO_2$and TiO_2. Meanwhile, Designs were made with the help of computer software which are called "Optilayer" and "MCalc" and the transmission and reflection measurements were done at room temperature.Coating processes have been done under 10^{-5} mbar chamber pressure and 150 $^{\circ}C$. Current value of E-beam gun is set 75 mA for the SiO_2 and 195 for the TiO_2. APS power is set 1.7 kw and coil current is set 1.38 Amper . Deposition rate is set 0.3 nm/sec for TiO_2 and 0.5 nm/sec for SiO_2.

4.2 Design of a Near Infrared Interference Filter

At the beginning target values are defined. Target values for our design are % 0 T in the spectral region 400 nm-700 nm and % 100 T in the spectral region 700 nm-1400 nm as shown on the Figure 4.1.

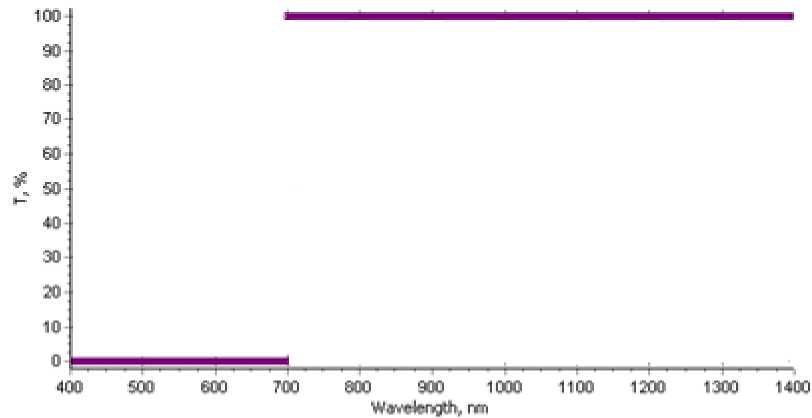

Figure 4.1: Target values on the software

After defining the target values, light source and detector are defined as shown on the Figure 4.2.

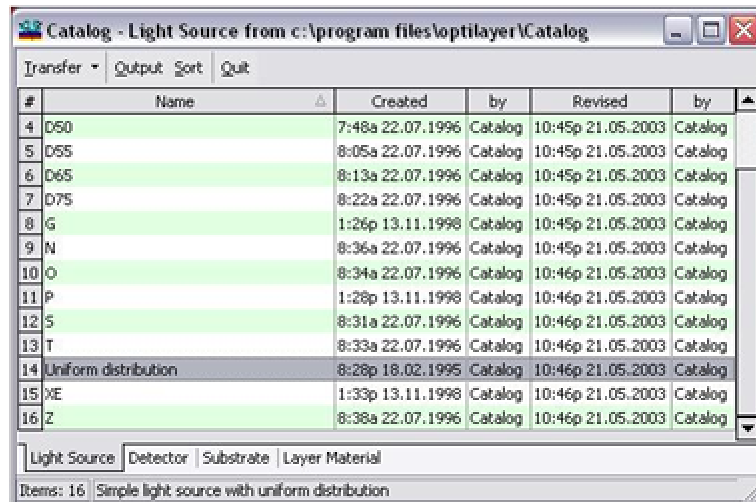

#	Name	Created	by	Revised	by
4	D50	7:48a 22.07.1996	Catalog	10:45p 21.05.2003	Catalog
5	D55	8:05a 22.07.1996	Catalog	10:45p 21.05.2003	Catalog
6	D65	8:13a 22.07.1996	Catalog	10:45p 21.05.2003	Catalog
7	D75	8:22a 22.07.1996	Catalog	10:45p 21.05.2003	Catalog
8	G	1:26p 13.11.1998	Catalog	10:45p 21.05.2003	Catalog
9	N	8:36a 22.07.1996	Catalog	10:45p 21.05.2003	Catalog
10	O	8:34a 22.07.1996	Catalog	10:46p 21.05.2003	Catalog
11	P	1:28p 13.11.1998	Catalog	10:46p 21.05.2003	Catalog
12	S	8:31a 22.07.1996	Catalog	10:46p 21.05.2003	Catalog
13	T	8:33a 22.07.1996	Catalog	10:46p 21.05.2003	Catalog
14	Uniform distribution	8:28p 18.02.1995	Catalog	10:46p 21.05.2003	Catalog
15	XE	1:33p 13.11.1998	Catalog	10:46p 21.05.2003	Catalog
16	Z	8:38a 22.07.1996	Catalog	10:46p 21.05.2003	Catalog

Figure 4.2: Light source database

After defining the light source and detector, substrate is defined with its n and k values depending on wavelength. B270 glass have been chosen as the substrate and it has been defined to the software as shown on the Figure 4.3.

Catalog - Substrate/Incident/Exit Medium from c:\program files\opt...

Transfer Output Sort Database: All Items Quit

#	Name	Created	by	Revised	by
1	ADC1	11:48p 12.10.2008	Catalog	11:51p 12.10.2008	Catalog
2	Air	12:39a 12.05.2003	Catalog	12:49a 12.05.2003	Catalog
3	Aluminum	11:21a 05.11.2007	Catalog	1:29p 05.11.2007	Catalog
4	B 270	1:40p 25.06.1998	Catalog	12:55p 20.07.2007	Catalog
5	BAC4	11:48p 12.10.2008	Catalog	11:50p 12.10.2008	Catalog
6	BACD11	11:48p 12.10.2008	Catalog	11:50p 12.10.2008	Catalog
7	BACD14	11:48p 12.10.2008	Catalog	11:50p 12.10.2008	Catalog
8	BACD15	11:48p 12.10.2008	Catalog	11:50p 12.10.2008	Catalog
9	BACD16	11:48p 12.10.2008	Catalog	11:50p 12.10.2008	Catalog
10	BACD18	11:48p 12.10.2008	Catalog	11:50p 12.10.2008	Catalog
11	BACD2	11:48p 12.10.2008	Catalog	11:50p 12.10.2008	Catalog
12	BACD4	11:48p 12.10.2008	Catalog	11:50p 12.10.2008	Catalog
13	BACD5	11:48p 12.10.2008	Catalog	11:50p 12.10.2008	Catalog

Light Source Detector Substrate Layer Material

Items: 898 Date: 2007-07-17 Author: Bte Bedampfungstechnik GmbH, Joerg Terhuerne Source: Schott

Figure 4.3: Substrate database

Then, coating materials are defined to the software. SiO_2, TiO_2 and MgF_2 have been chosen as the coating materials as shown on the Figure 4.4.

Database - Layer Material

Load Edit New Copy Rename Delete Output Sort Quit

#	Name	Created	by	Revised	by
1	Ag (110-800nm, RIT)	8:27p 22.10.2008	Catalog	9:19p 24.10.2008	Catalog
2	MgF2	1:31p 15.08.2001	User	2:55p 24.10.2006	User
3	Ni (151-800nm, RIT)	8:27p 22.10.2008	Catalog	9:21p 24.10.2008	Catalog
4	Si3N4 (150-800nm, RIT)	8:27p 22.10.2008	Catalog	2:44a 23.10.2008	Catalog
5	SiO2 SyPro-P4433	1:31p 15.08.2001	User	10:35a 03.06.2009	User
6	TiO2 SyPro-P4433	3:37p 06.11.2001	User	10:35a 03.06.2009	User

Target Color Target Light Source Detector Cone Angle Substrate Layer Material Design

Items: 6

Figure 4.4: Layer materials database

After that, initial design can be created. Initial design has a crucial importance to decrease the number of layers as possible as because initial design makes the optimization easy according to the situation. The purpose of the optimization is to reach target values. Many Near Infrared Interference filters have been designed during the thesis work and linear refinement and needle optimization techniques have been used for the optimization. One of the initial designs is shown on the Figure 4.5.

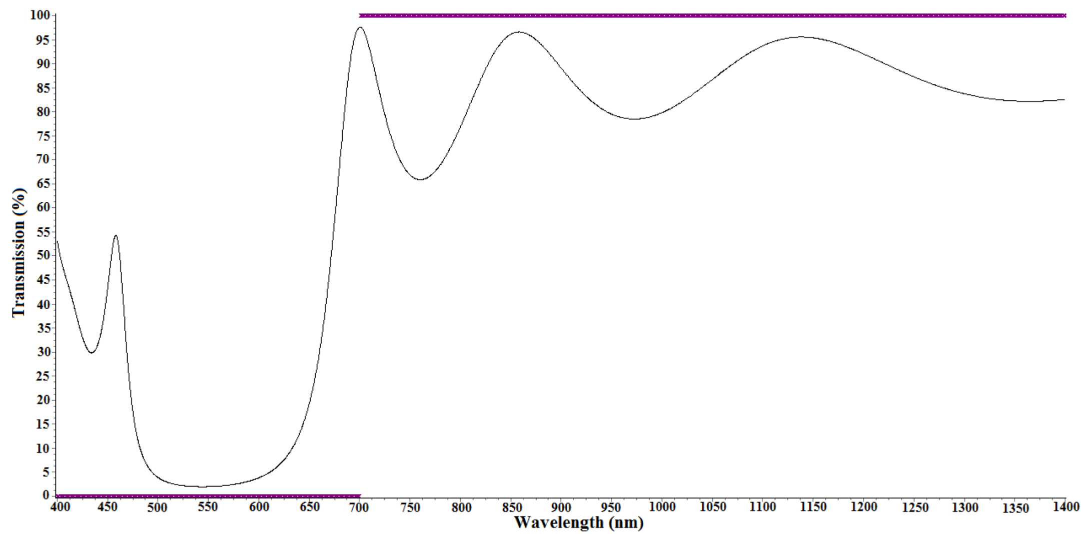

Figure 4.5: Initial design for NIR interference filter

After making refinement design becomes as the Figure 4.6.

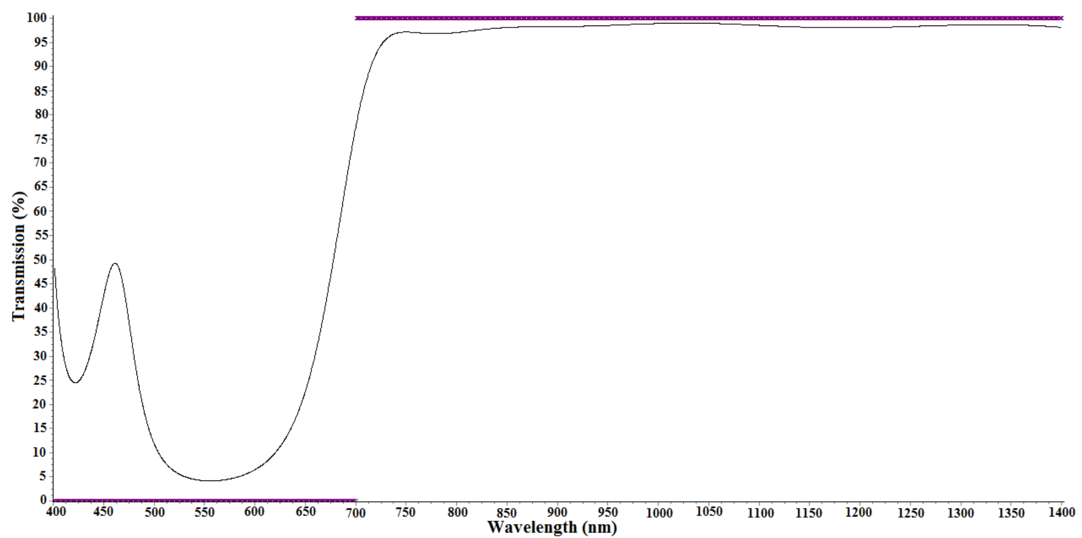

Figure 4.6: Initial design after applying refinement

After applying needle optimization the design that is shown on the Figure 4.7 is obtained. For this design, $TiO_2$is used as a high refractive index material and SiO_2 is used as a low index material. Design consists of 31 layers and average transmission values are shown on the Figures 4.7 and Table 4.8.

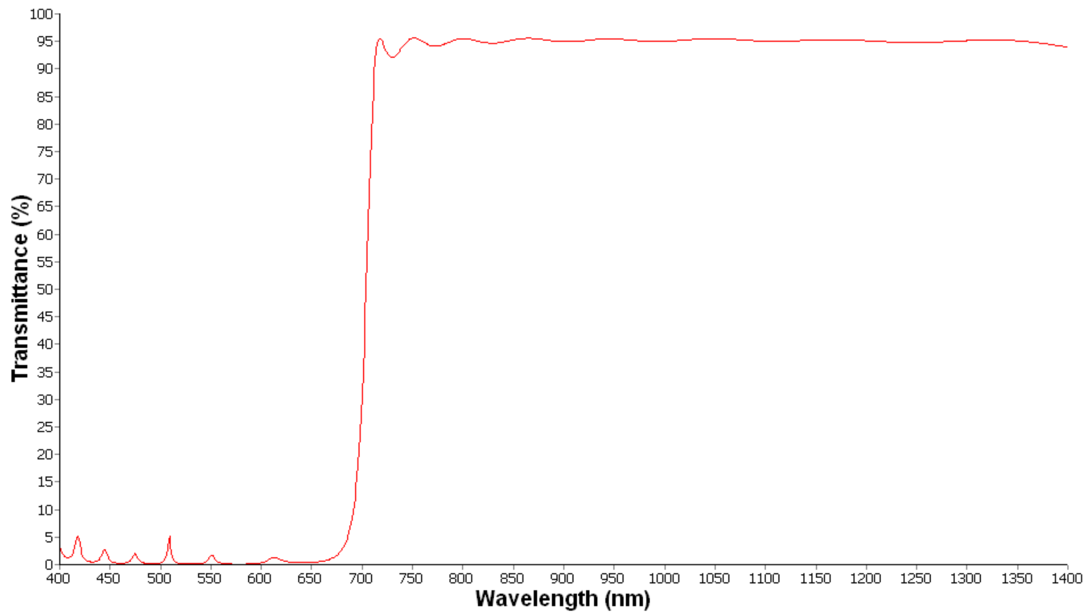

Figure 4.7: Transmission of designed 31 layer NIR interference filter with backside reflections

Table 4.1: Average transmission value of the designed 31 layer NIR interference filter with backside reflections

	400nm-680nm	720nm-1400nm
Transmission(%)	0.82	95.03

4.3 Homogeneity Studies

Production processes of the optical filters have been done with the optical coating system that is shown on the Figure 4.8. Before the productions, homogeneous deposition of the coating materials must be ensured. If surface of the substrate holder is flat there is not a homogeneity problem. However, if substrate holder has a curved surface, thickness of coated material on the each substrate is different. Therefore, homogeneity studies have been done awhile before the productions of the designed optical filters.

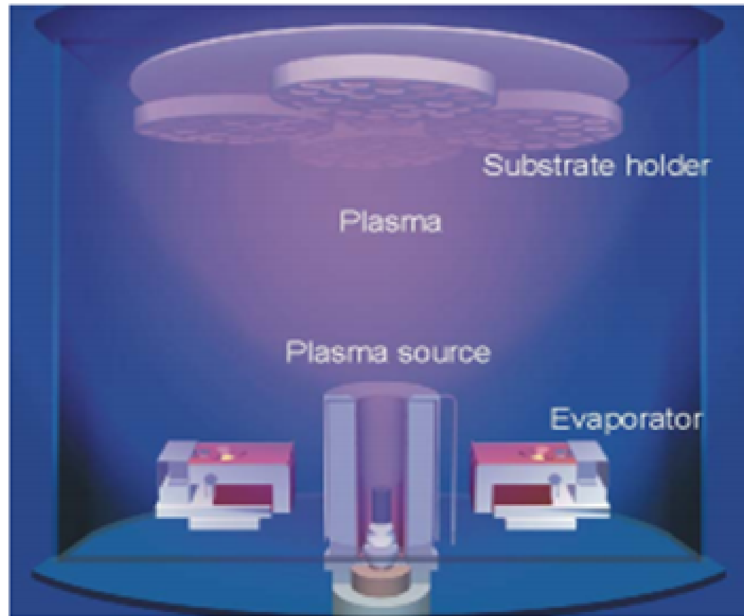

Figure 4.8: Optical Coating System

The substrate holder that is shown on the Figure 4.9 has nine different positions and while coating process it is rotating around itself to make the homogeneity better. Although the substrate holder is rotating, homogeneity is still not same exactly. The Figure 4.10 shows reflection curves of produced single layer SiO_2 for three different substrate positions and it can be easily seen that homogeneity is not same for these substrates.

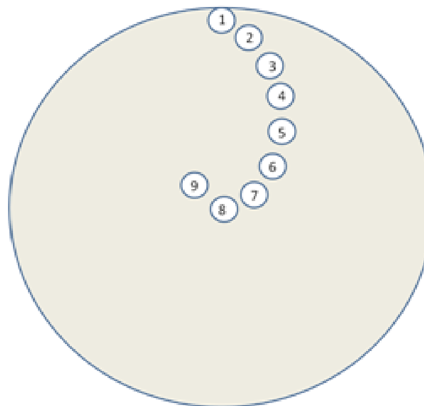

Figure 4.9: Substrate positions on the substrate holder

Physical thicknesses of the coated material on the substrates that are on the different positions can be found from the transmission (or reflection) curves of the substrates.Figure 4.10 shows that a single layer SiO_2 have been coated to see the delivery of coating material.Because of the relative reflection, reflection exceeds % 100. Depending on the physical thicknesses, the shape of homogeneity mask is determined. Therefore, homogeneity mask

that is shown on the Figure 4.11 has been shaped.

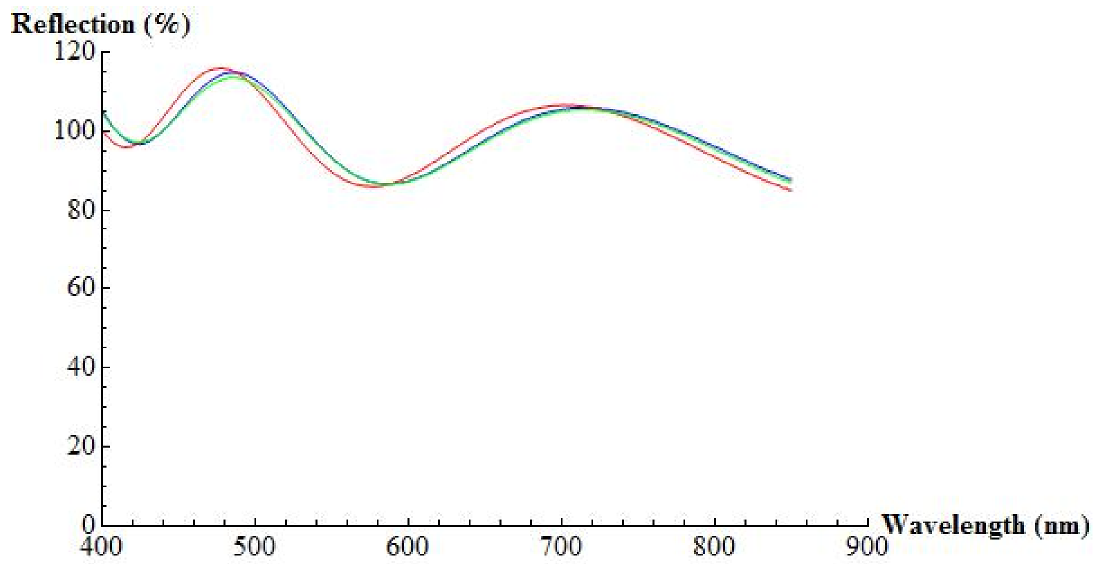

Figure 4.10: Reflection of single layer SiO_2

Figure 4.11: Substrate holder with homogeneity mask

4.4 Production and Analysis of the Near Infrared Interference Filter with OMS

Firstly, transmission and reflection of the substrates that will be coated on have been measured and data that is shown on the Figure 4.12 and 4.13 has been obtained.

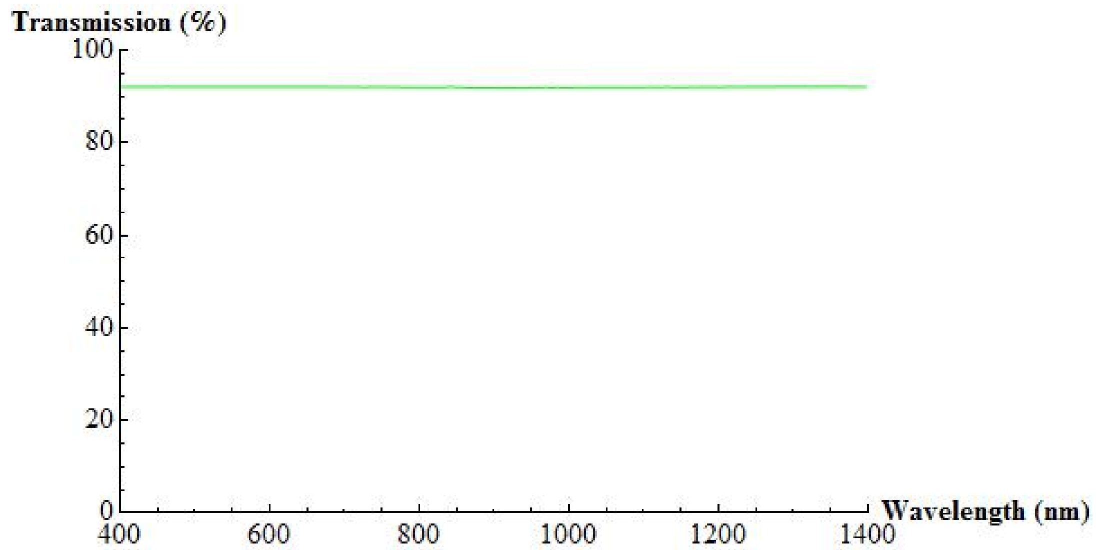

Figure 4.12: Transmission of uncoated glass(B270)

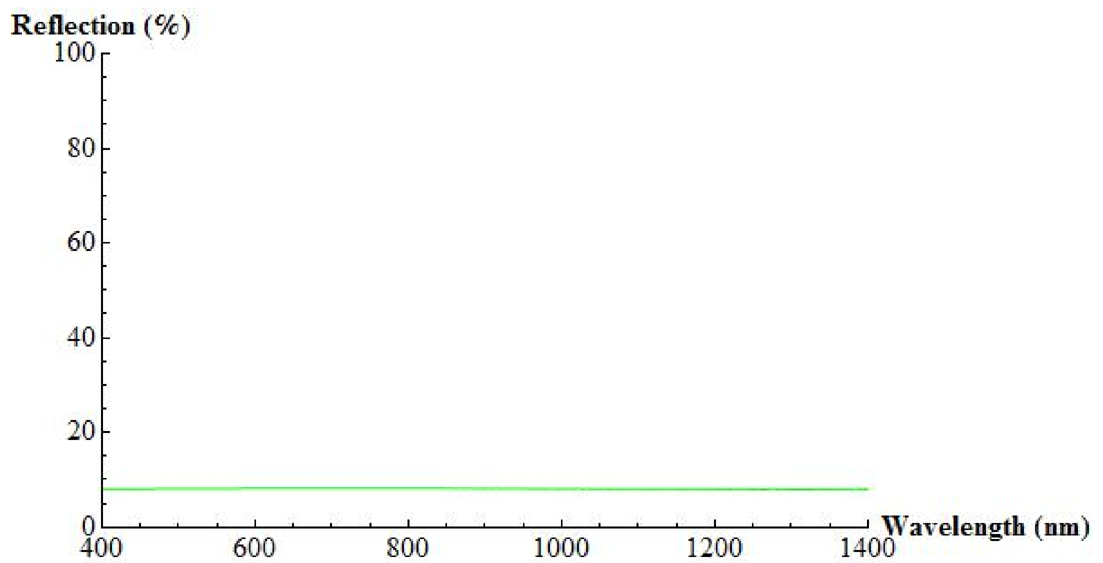

Figure 4.13: Reflection of uncoated glass(B270)

Then, design that is shown on the Figure 4.7 has been coated and transmission spectrum that is shown on the Figure 4.14 has been obtained. While coating the substrate, OMS has been used as the measurement unit.

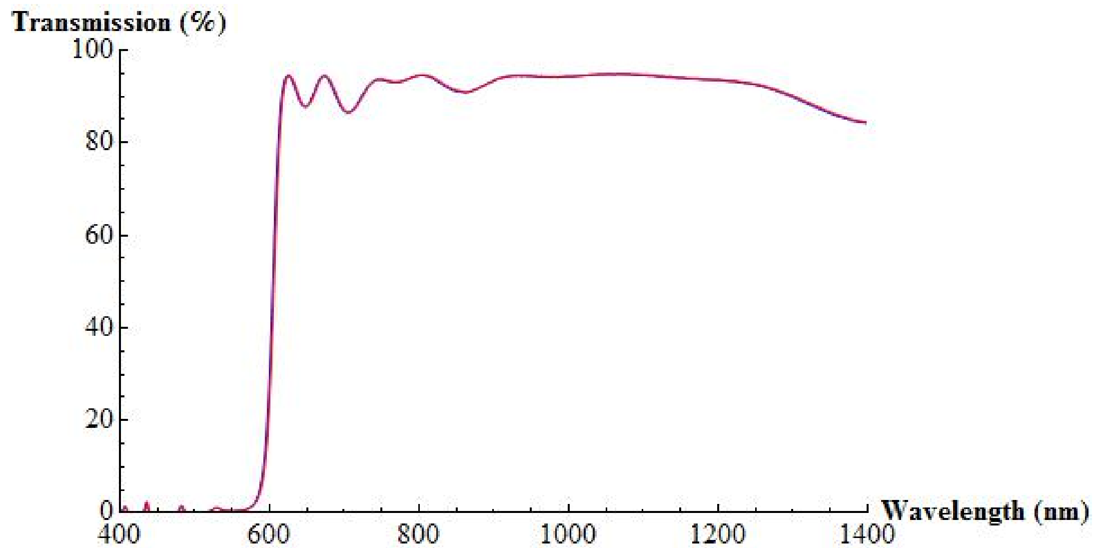

Figure 4.14: Transmission of measured 31 layer NIR interference filter with backside reflections

Because of the difference of distance between measurement units and substrates, coating thickness for each material is not same on the substrates as designed coating. As a result of this situation, the thickness of each material that is used in the design should be multiplied by a constant which is called tooling factor. In order to calculate the tooling factor for each material, single layer titanium dioxide and silicon dioxide was coated on the B270 glass and spectrum measurement results are given on the Figures 4.15 and 4.16.

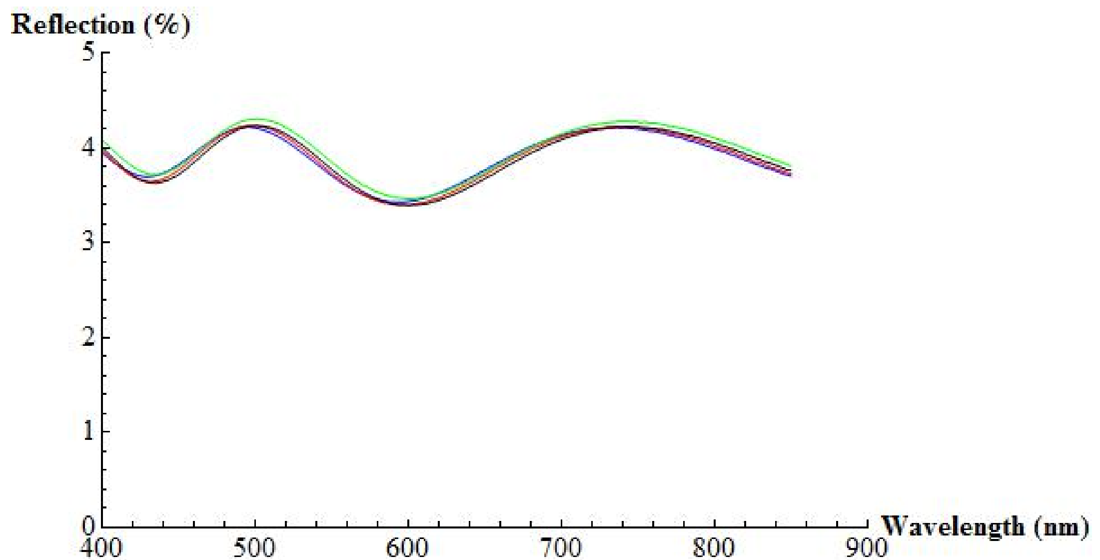

Figure 4.15: Reflection of measured single layer SiO_2

If we know the reflection vs wavelength we can find the refractive index of the coating material by using the equation as follows;

$$n_{layer} = \sqrt{n_{substrate}\frac{1 + \sqrt{R}}{1 - \sqrt{R}}} \tag{4.1}$$

At the $5\lambda/4$ point,

$\lambda = 592.5$, $R = 3.43$

Therefore, $n = 1.486$

This is almost same with the value of production.

$$nd = m\lambda/4 \implies \qquad d = \frac{m\lambda}{4n} \tag{4.2}$$

$d_{coating} = 497.98$ nm, $d_{xms} = 482$ nm

Tooling for quartz crystal;

$$T_{new} = T_{old} \times \frac{d_{actual}}{d_{input}} \implies \qquad T_{SiO_2} = \%103.3 \tag{4.3}$$

Tooling for OMS;

$$T_{old} = \frac{d_{testglass}}{d_{substrate}} \qquad \implies \qquad T_{SiO_2} = \frac{5.1 \times 645nm}{5.0 \times 592nm} = \%111.1 \tag{4.4}$$

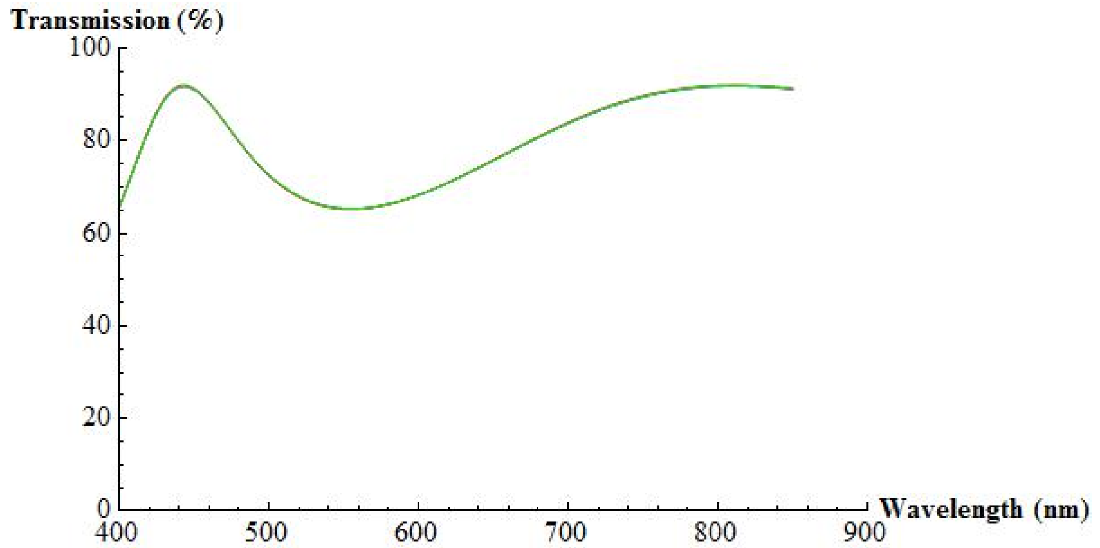

Figure 4.16: Transmission of measured single layer TiO_2

If we have transmission vs wavelength graph we can calculate refractive index of the coating material by using the equation as follows,

$$r_1 = \left(\frac{1 - n_{substrate}}{1 + n_{substrate}}\right) \tag{4.5}$$

$$r_2 = \frac{1 - r_1 - T}{1 - r_1(1 + T)} \tag{4.6}$$

r_1; reflection of the uncoated testglass, r_2; reflection of the coated testglass.

$$n_{layer} = \sqrt{n_{substrate}\frac{1 + \sqrt{r_2}}{1 - \sqrt{r_2}}} \tag{4.7}$$

Refractive index of coating material is calculated by using data on the Figure 4.16.

$\lambda = 556nm$, $T = 65.31$ $(n = 2.363)$

$nd = m\lambda/4 \quad \Longrightarrow \quad d_{coating} = 176.47nm$

Tooling for quartz crystal ;

$$T_{new} = T_{old} \times \frac{d_{actual}}{d_{input}} \quad \Longrightarrow \quad T_{SiO_2} = \%101.15$$

Tooling for OMS;

$$T_{old} = \frac{d_{testglass}}{d_{substrate}} \quad \Longrightarrow \quad T_{SiO_2} = \frac{3.1 \times 645nm}{3.0 \times 556nm} = \%119.8$$

After calculating the tooling factor for both quartz crystal and OMS, the same design was again produced. In this time, each layer thickness was multiplied by tooling factor. Transmission of the coated substrates have been measured by spectrophotometer and results are shown on the Figure 4.17.

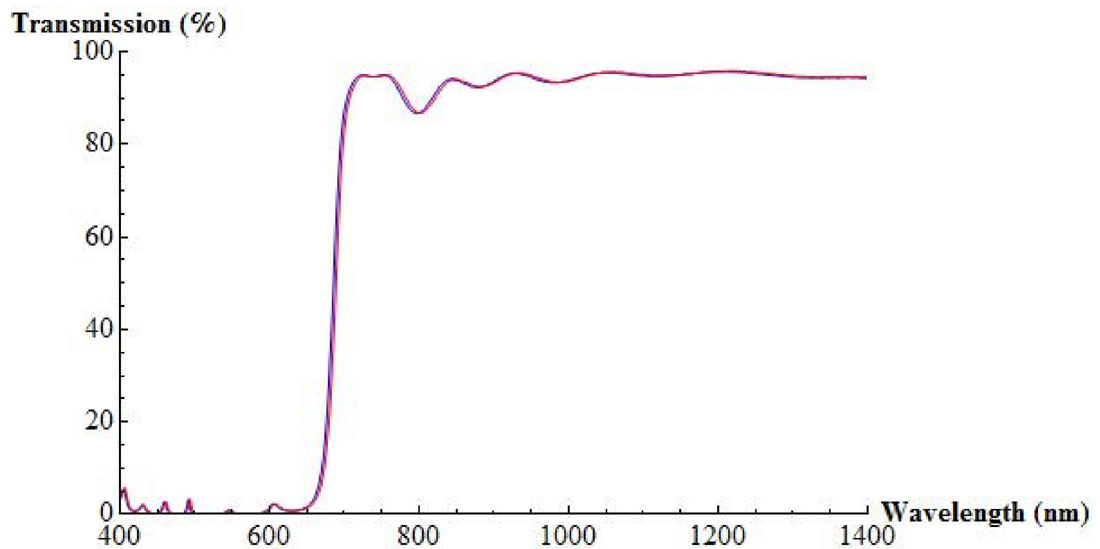

Figure 4.17: Transmission of measured 31 layer NIR interference filter with backside reflections

Reflection spectrum of the designed filter is shown on the Figure 4.18, average reflection values of designed filter are shown on the Table 4.2 and reflection spectrum of the coated substrates is shown on the Figures 4.19 .

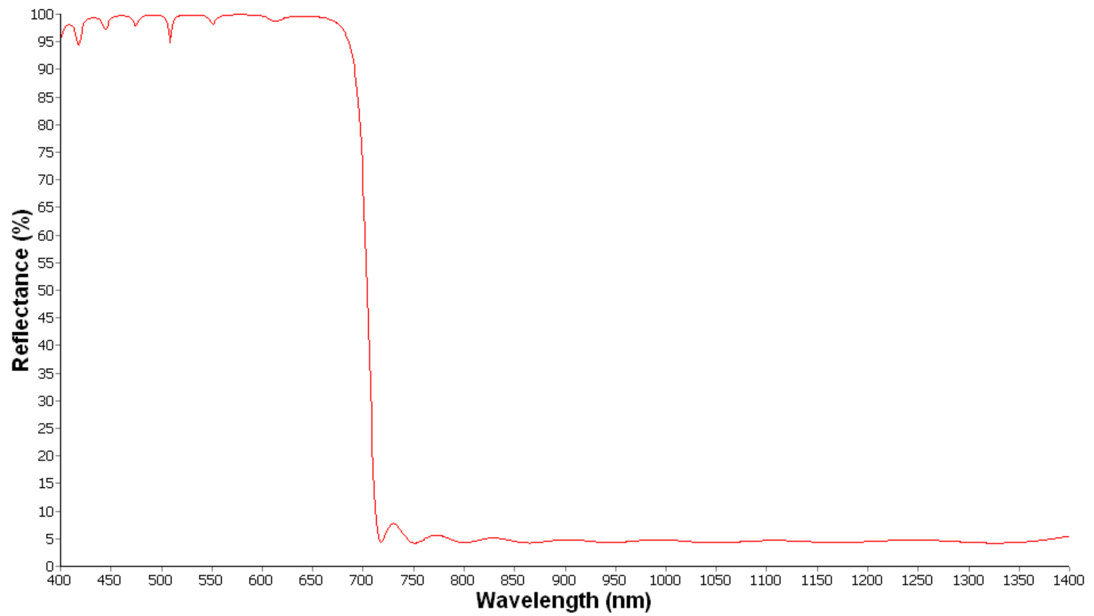

Figure 4.18: Reflection of designed 31 layer NIR interference filter with backside reflections

Table 4.2: Average reflection values of the designed 31 layer NIR interference filter with back side reflections

	400nm-680nm	720nm-1400nm
Reflection(%)	99.10	4.66

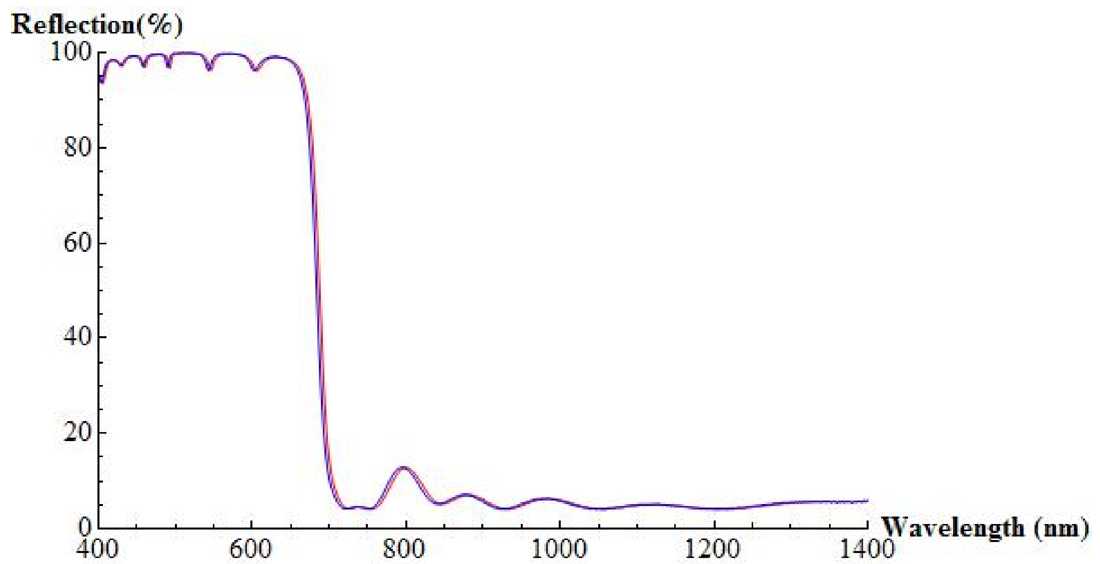

Figure 4.19: Reflection of measured 31 layer NIR interference filter with backside reflections

Because of the reflections from backside of substrate, transmission is decreased almost %4. To solve this problem, antireflection coating is designed for back side of the substrate. This back side design has five layers and SiO_2 and TiO_2 have been used as the low and high

index materials. Transmission of designed 31 layer NIR interference filter with backside antireflective coating design is shown on the Figure 4.20.

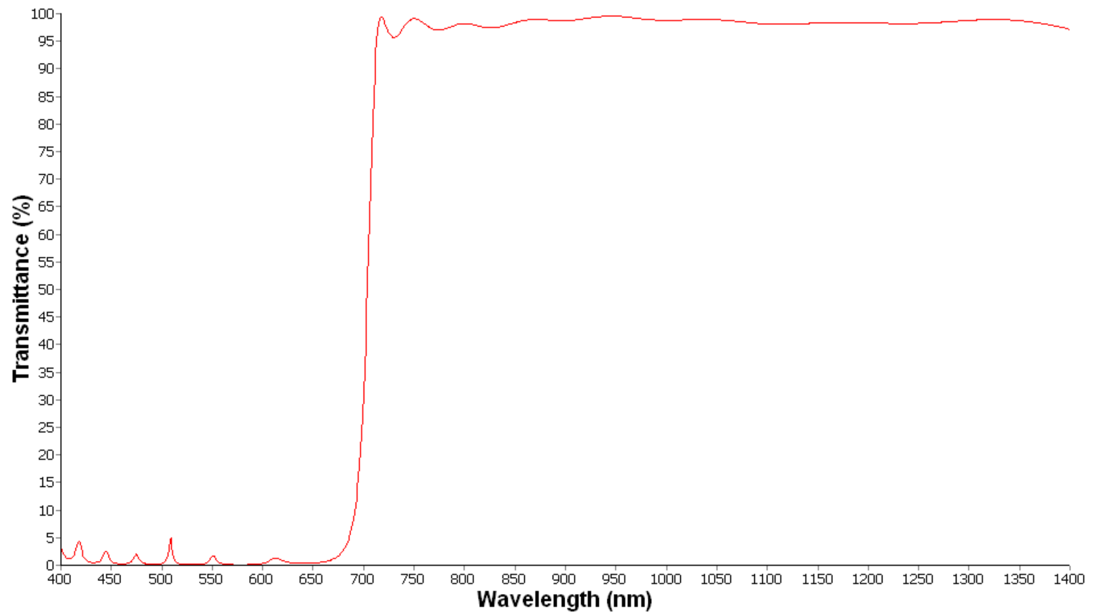

Figure 4.20: Transmission of designed 31 layer NIR interference filter with backside antireflective coating design

Table 4.3: Average transmission values of the designed 31 layer NIR interference filter with back side antireflective coating design

	400nm-680nm	720nm-1400nm
Transmission(%)	0.80	98.44

After coating backside of the substrate, transmission vs wavelength graph that is shown on the Figure 4.21 has been obtained.

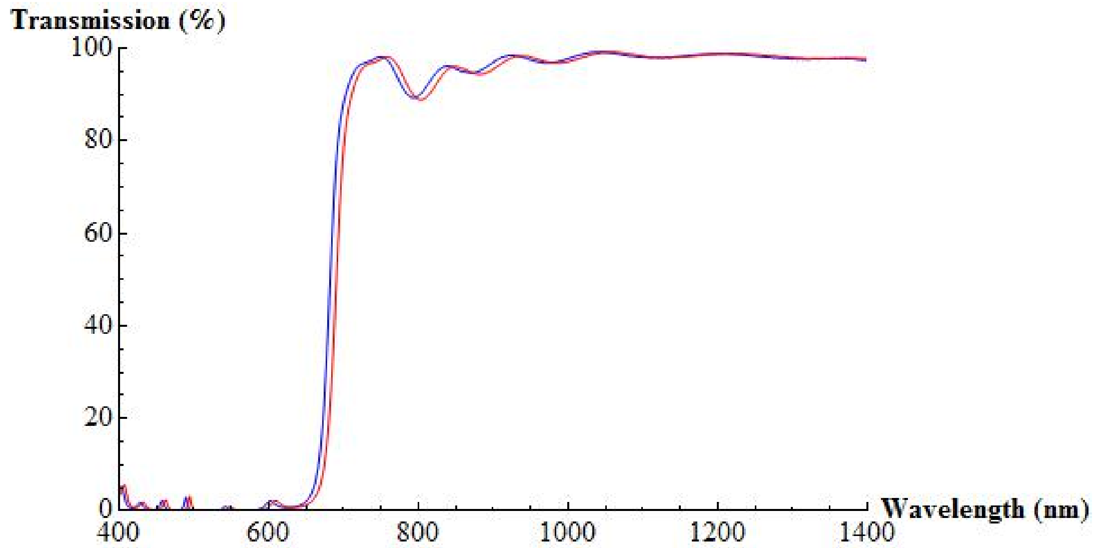

Figure 4.21: Transmission of measured 31 layer NIR interference filter with backside antireflective coating

Reflection spectrum for the same design is shown on the Figure 4.22 and average reflection data is shown on the Table 4.4.

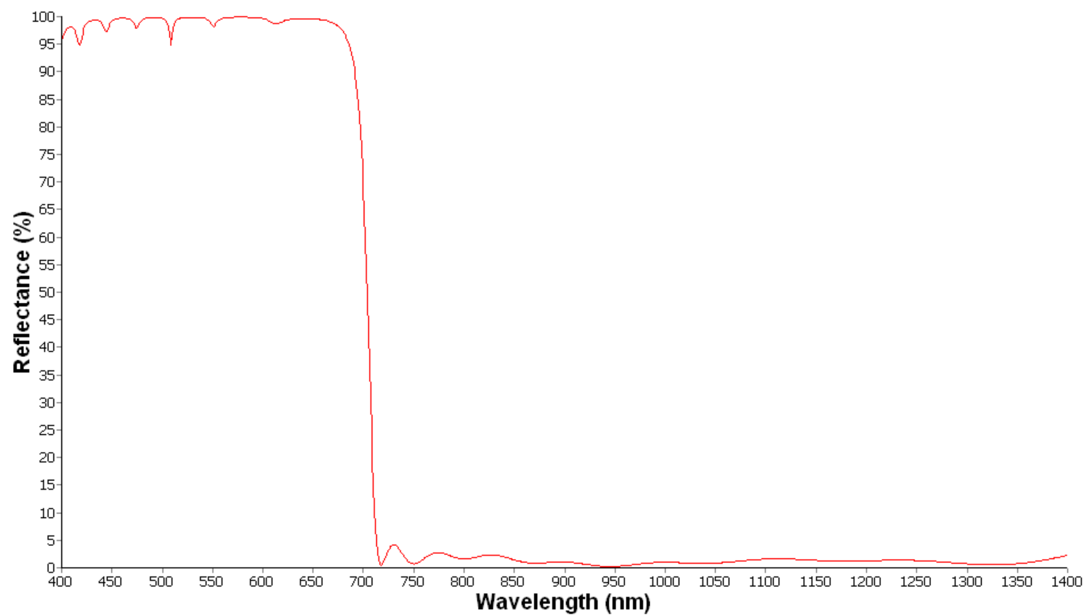

Figure 4.22: Reflection of designed 31 layer NIR interference filter with backside antireflective coating design

Table 4.4: Average reflection values of the designed 31 layer NIR interference filter with back side antireflective coating design

	400nm-680nm	720nm-1400nm
Reflection(%)	99.11	1.26

Reflection spectrum of the produced near infrared interference filter is shown on the Figure 4.23.

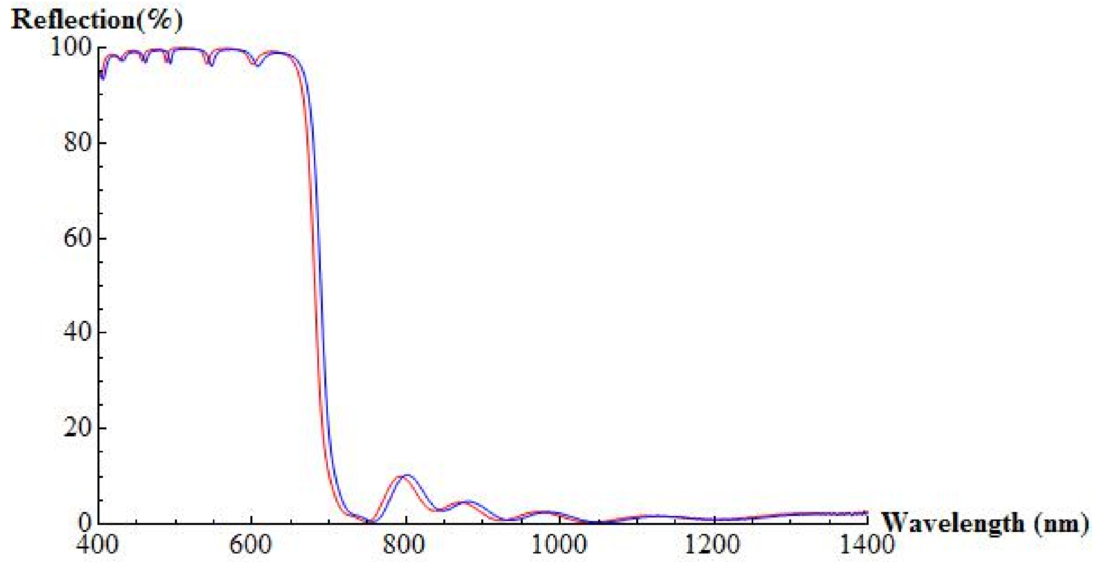

Figure 4.23: Reflection of measured 31 layer NIR interference filter with backside antireflective coating

4.5 Production and Analysis of the Near Infrared Interference Filter with Quartz Crystal

Another design of the Near Infrared Interference filter is shown on the Figure 4.24 SiO_2 and TiO_2 have been used as the low and high refractive index materials for this design. This design consists of 27 layers and average transmission values are shown on the Table 4.5.

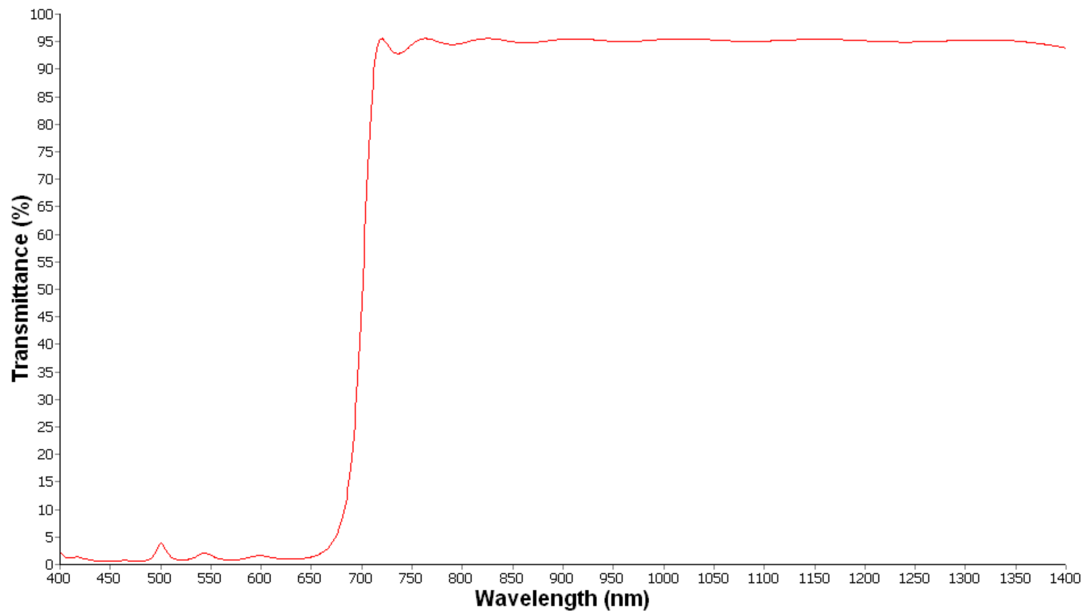

Figure 4.24: Transmission of designed 27 layer NIR interference filter with backside reflections

Table 4.5: Average transmission values of the designed 27 layer NIR interference filter with back side antireflective coating design

	400nm-680nm	720nm-1400nm
Transmission(%)	1.42	95.10

Transmission spectrum of the produced 27 layer Near Infrared Interference filter is shown on the Figure 4.25. While coating the substrate, quartz crystal has been used as the measurement unit.

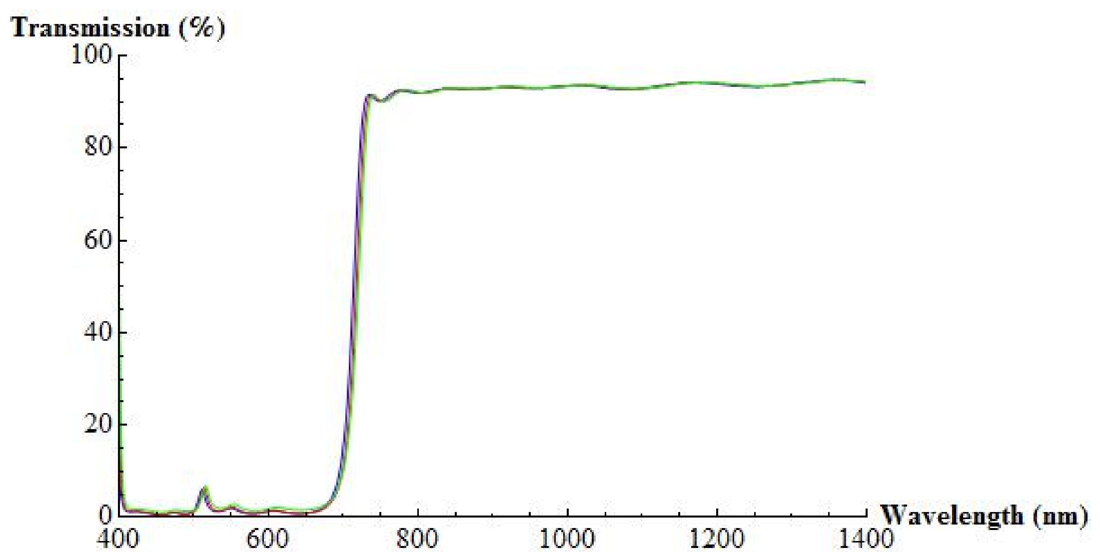

Figure 4.25: Transmission of measured 27 layer NIR interference filter with backside reflections

Reflection spectrum of the designed 27 layer NIR interference filter is shown on the Figure 4.26 and average reflection values are shown on the Table 4.6

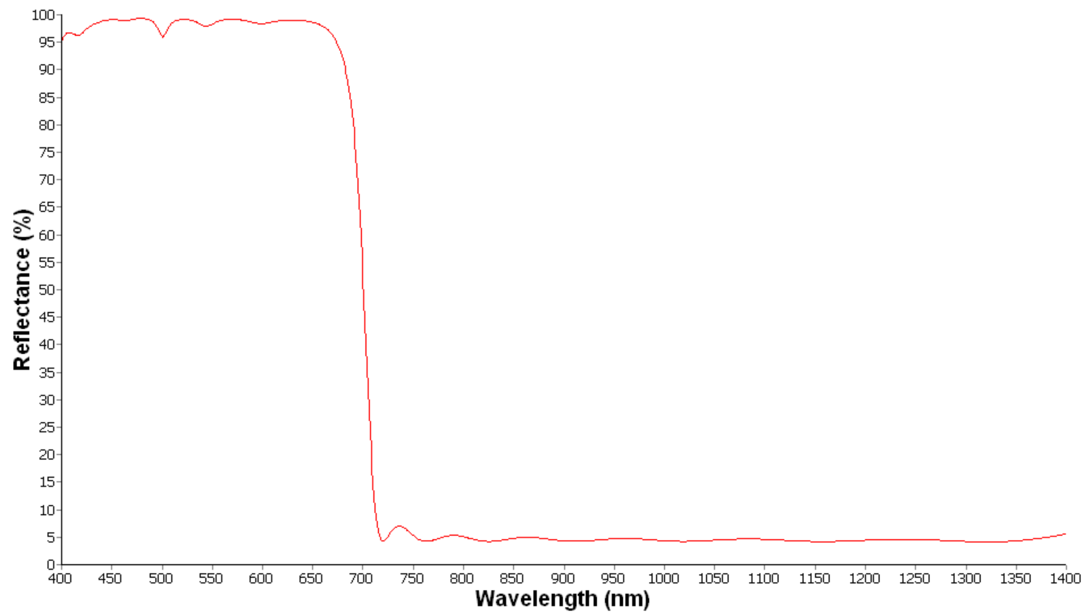

Figure 4.26: Reflection of designed 27 layer NIR interference filter with backside reflections

Table 4.6: Average reflection values of the designed 27 layer NIR interference filter with back side reflections

	400nm-680nm	720nm-1400nm
Reflection(%)	98.29	4.59

When reflection of the produced filter was measured the spectrum that is shown on the Figure 4.27 was obtained.

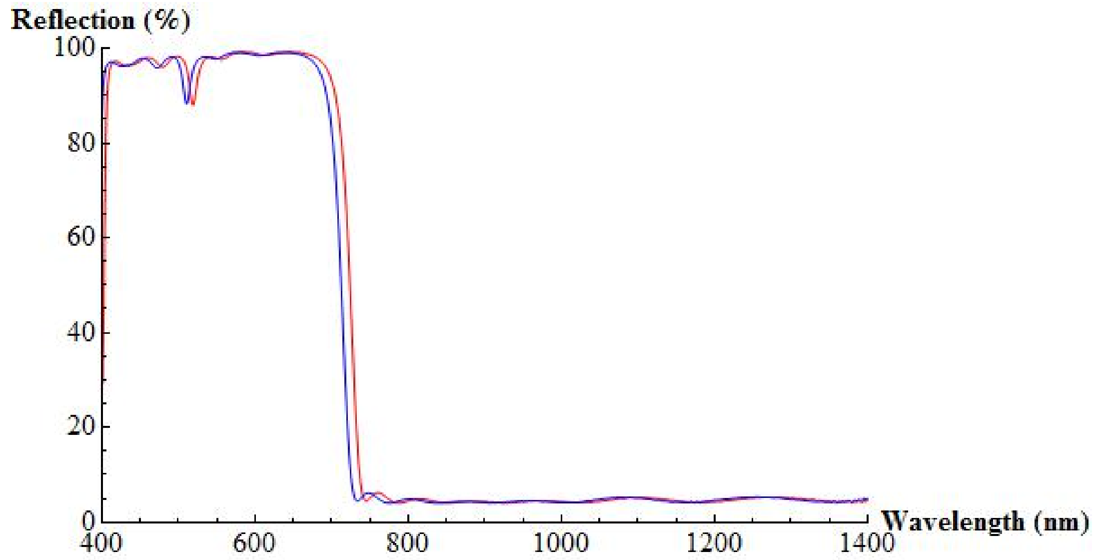

Figure 4.27: Reflection of measured 27 layer NIR interference filter with backside reflections

To prevent the backside reflections, 5 layer antireflective coating was designed and this design was added as the back side antireflective coating. After adding the backside antireflective coating design became as Figure 4.28 and its average transmission values are shown on the Table 4.7.

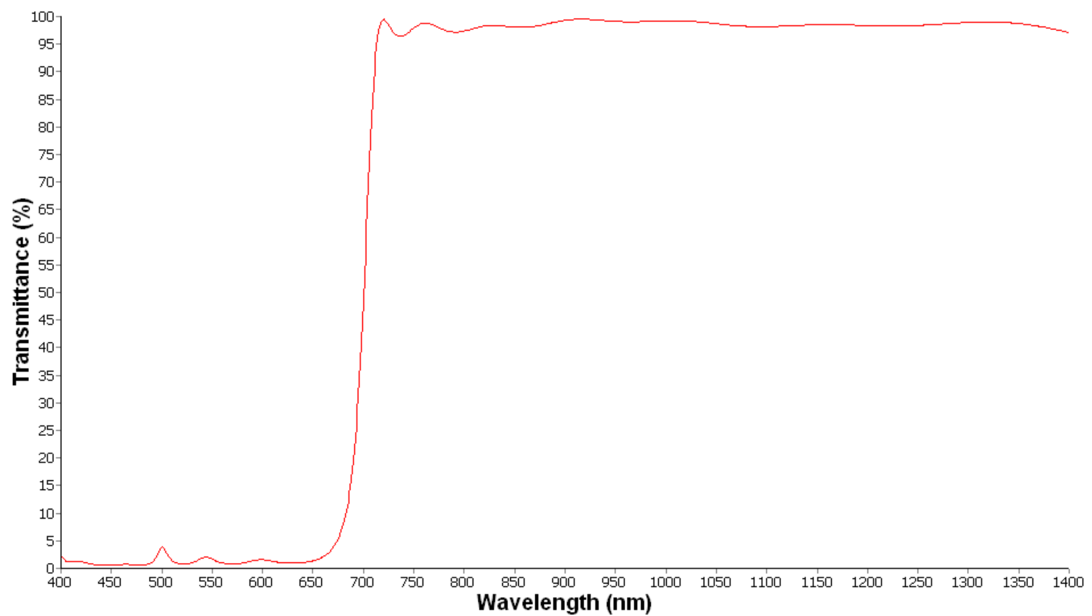

Figure 4.28: Transmission of designed 27 layer NIR interference filter with backside antireflective coating design

Table 4.7: Average transmission values of the designed 27 layer NIR interference filter with backside antireflective coating design

	400nm-680nm	720nm-1400nm
Transmission(%)	1.41	98.51

As back side of the substrate that had been coated 27 layer was coated with antireflective coating the spectrum shown on the Figure 4.29 was obtained.

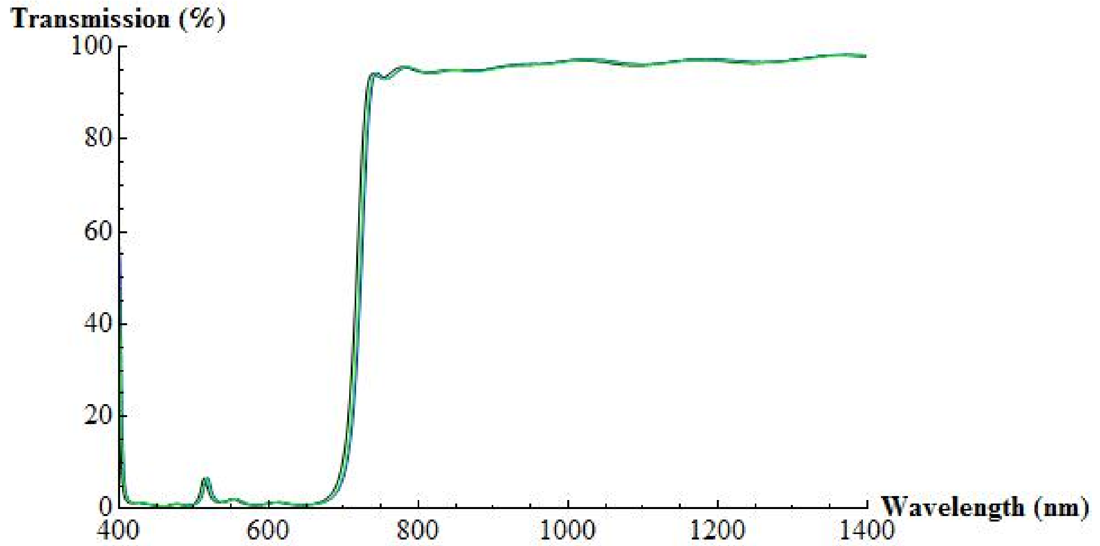

Figure 4.29: Transmission of measured 27 layer NIR interference filter with backside antireflective coating

4.6 Angle of Incidence Analysis

When the angle of incidence is different from zero, it is investigated that how the transmission spectrum is changed. Hence, transmission spectrum is obtained as shown on the Figures 4.30, 4.31, 4.32 and 4.33 under different angles of incidence.

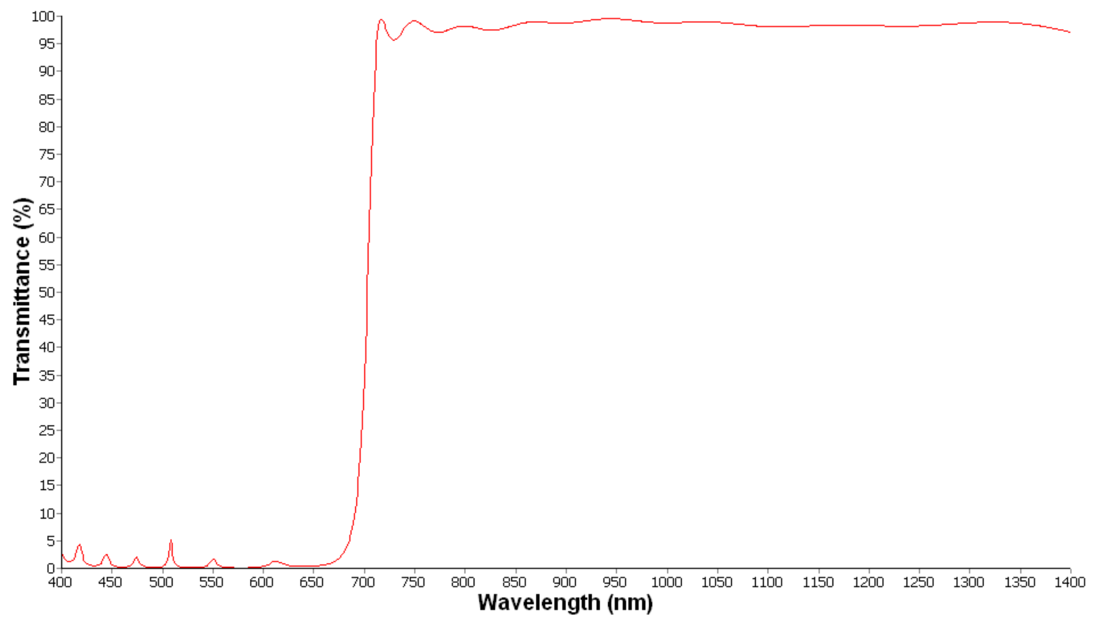

Figure 4.30: Transmission of designed 31 layer NIR interference filter with 5° angle of incidence

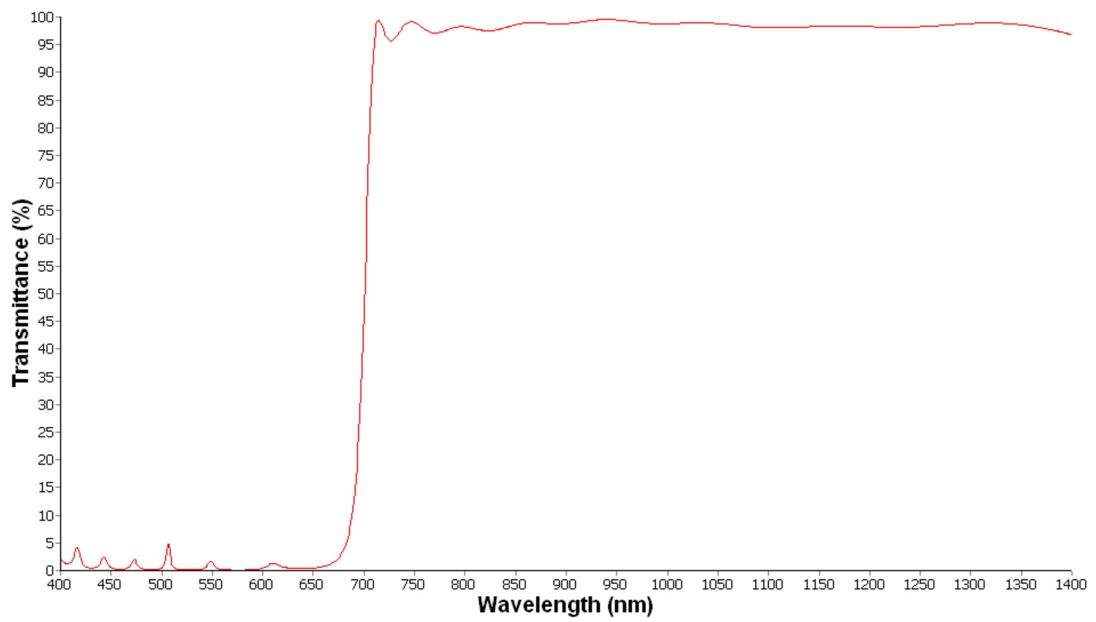

Figure 4.31: Transmission of designed 31 layer NIR interference filter with 10° angle of incidence

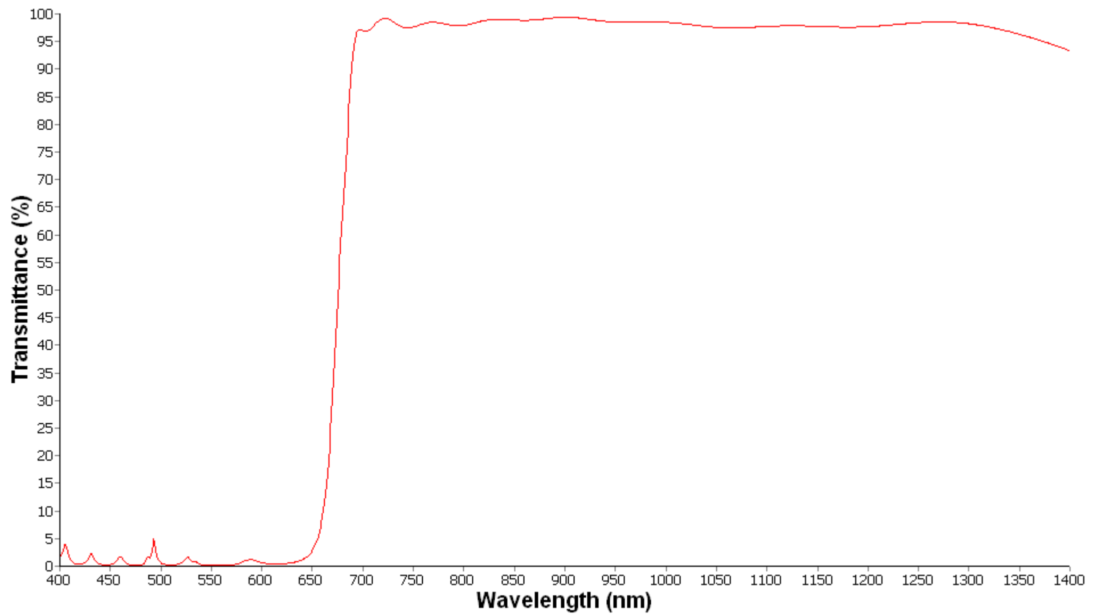

Figure 4.32: Transmission of designed 31 layer NIR interference filter with 30° angle of incidence

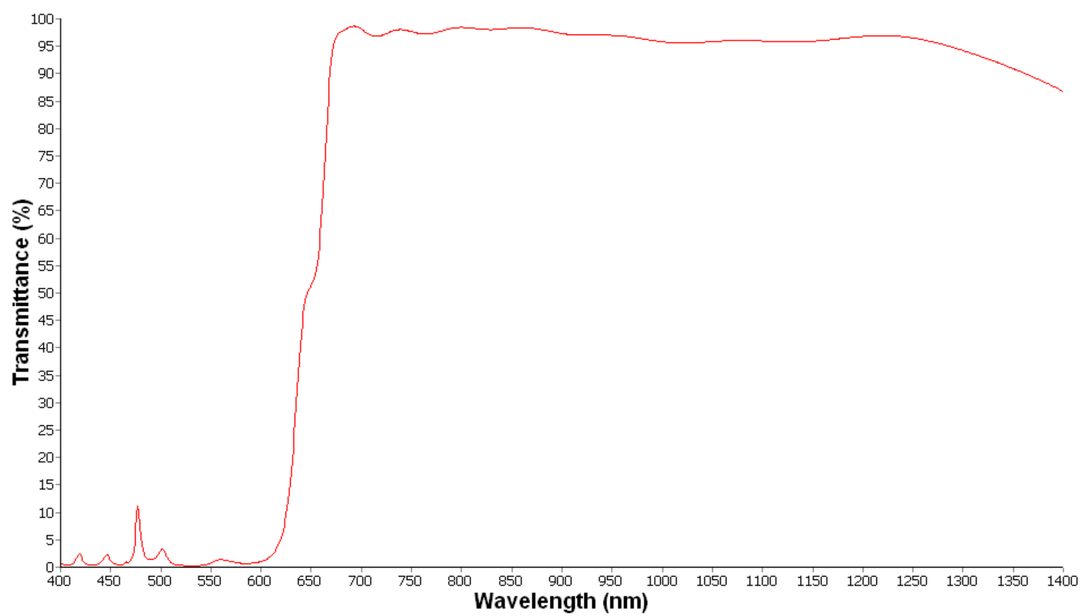

Figure 4.33: Transmission of designed 31 layer NIR interference filter with 45° angle of incidence

In the same way, when transmission spectrum of the designed 27-layer NIR interference filter is investigated under different angle of incidence the transmission values shown on the Figures 4.34, 4.35, 4.36 and 4.47 are obtained.

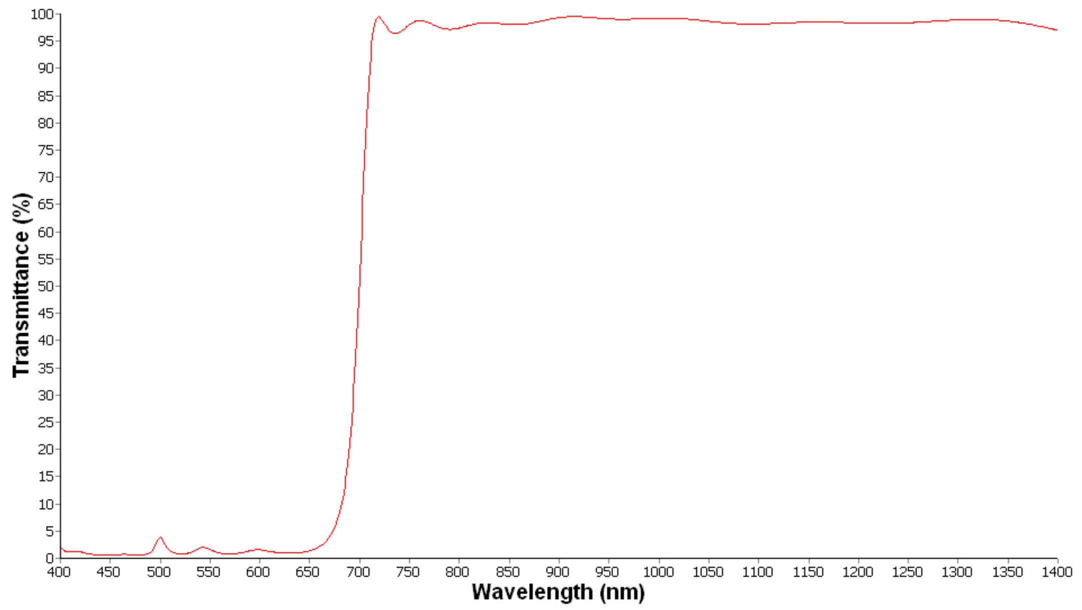

Figure 4.34: Transmission of designed 27 layer NIR interference filter with 5° angle of incidence

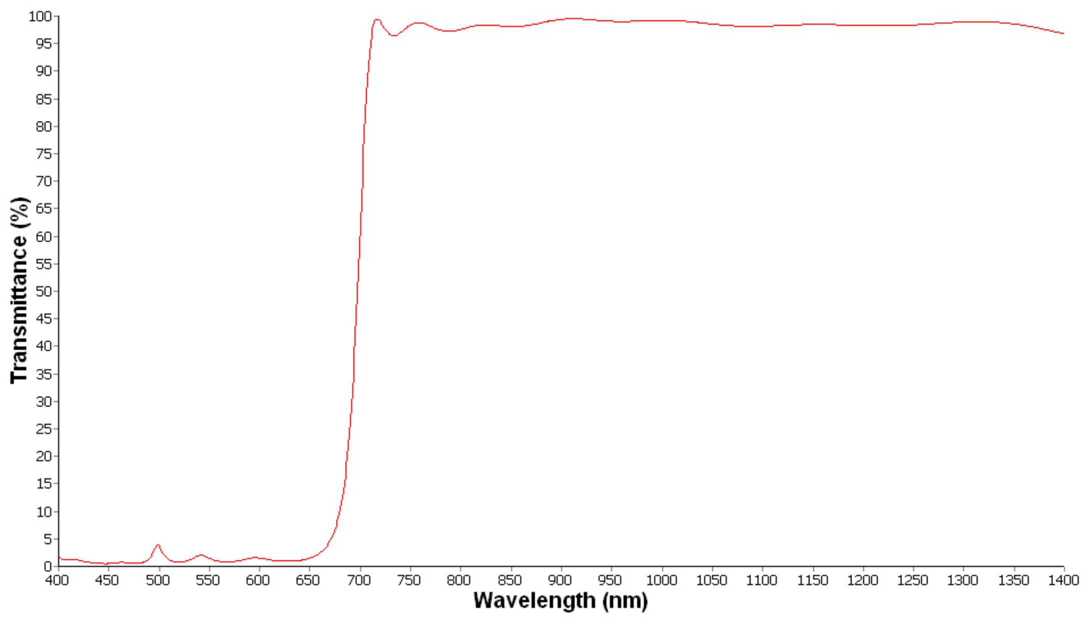

Figure 4.35: Transmission of designed 27 layer NIR interference filter with 10° angle of incidence

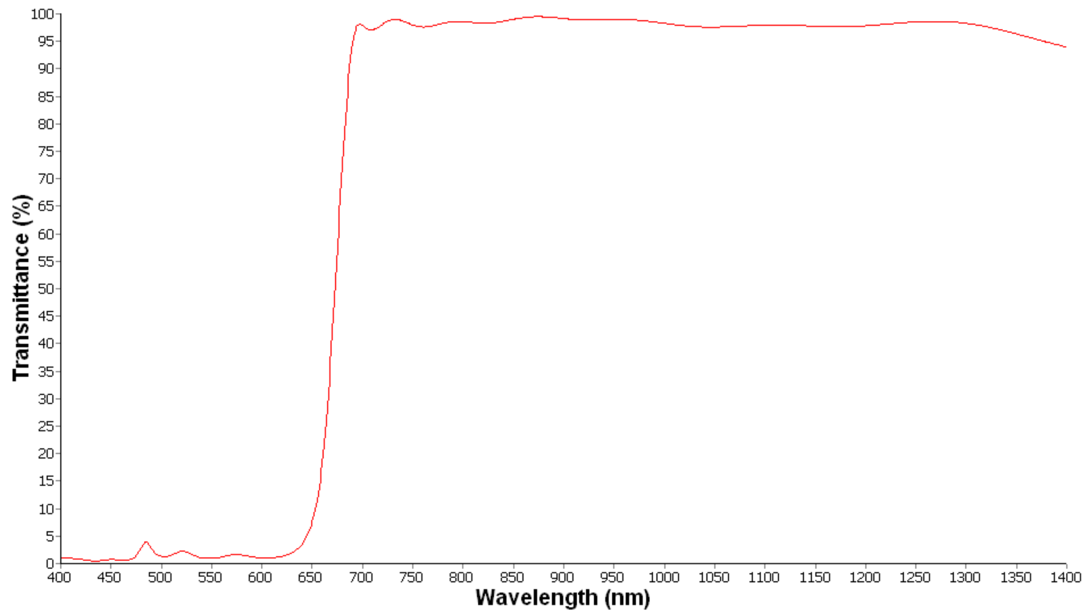

Figure 4.36: Transmission of designed 27 layer NIR interference filter with 30° angle of incidence

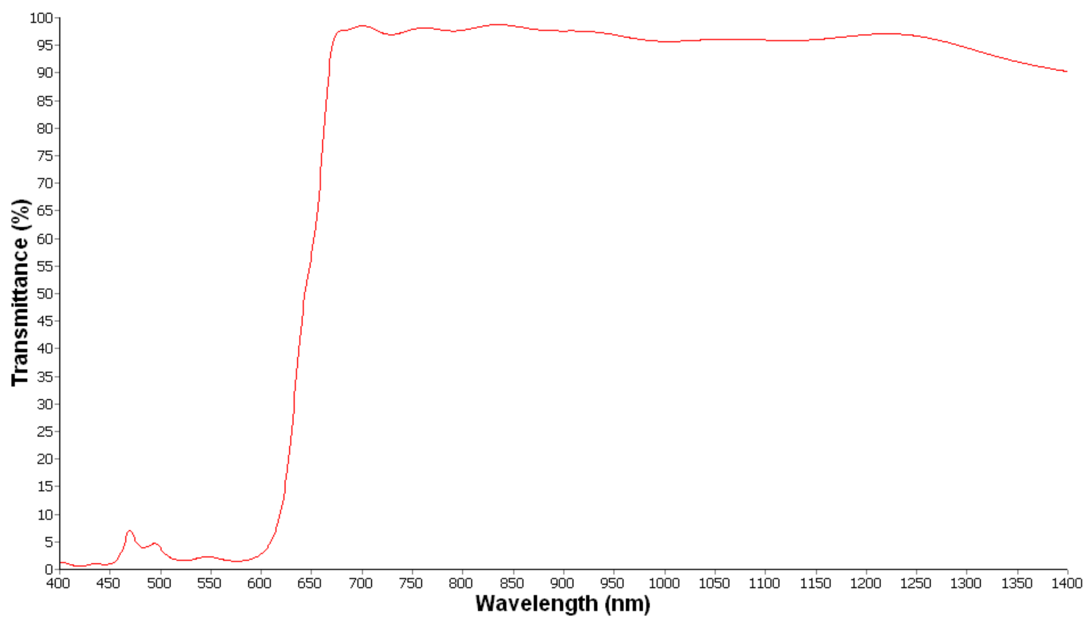

Figure 4.37: Transmission of designed 27 layer NIR interference filter with 45° angle of incidence

4.7 Durability Analysis

Transmittance spectra of the produced filters were measured and evaluated again after three months to look at the quality of durability. The two samples of transmittance spectra are shown on the Figure 4.38 and average transmission values are shown on the Table 4.8. There

is an increment almost %0.74 in the spectra region of 400-680 nm and there is a decrease almost %0.94 in the spectra region of 720-1400 nn. These increasing and decreasing are result of the mechanical stress between the coating materials.

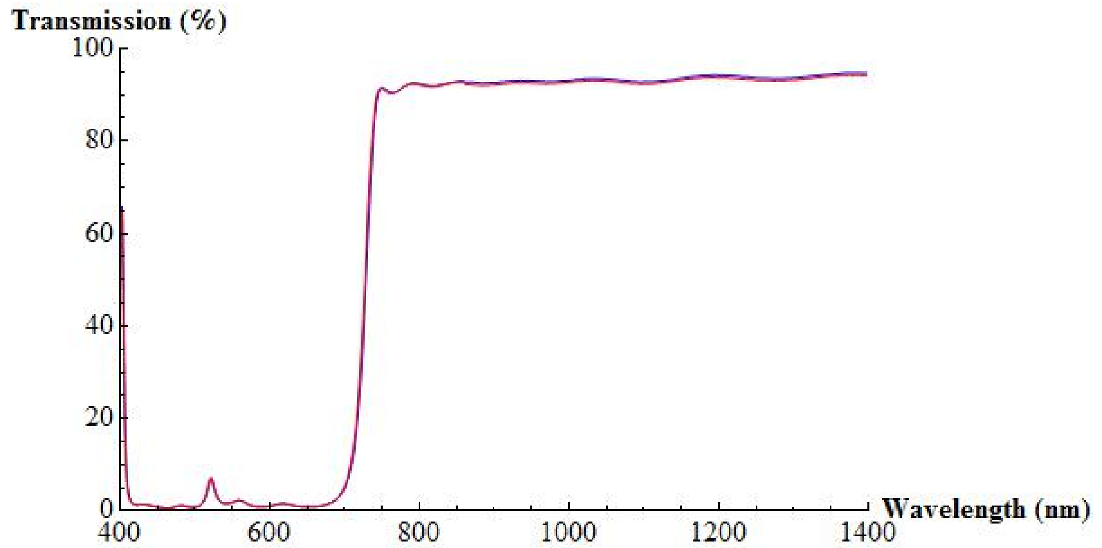

Figure 4.38: Transmission spectrum after three months

Table 4.8: Transmission values of two samples after transmission and three months after production

Filter	Transmission values after production		Transmission after three months	
	400-680 nm	720-1400 nm	400-680 nm	720-1400 nm
Sample 1	% 2.5	% 92.8	% 2.8	% 92.1
Sample 2	% 1.7	% 93.0	% 2.7	% 91.8

CHAPTER 5

CONCLUSION

In this thesis work, we have aimed to design and produce a Near infrared interference filter that blocks the visible spectrum region and transmits the near infrared spectrum region. For this purpose, thin film theory and optical coating methods have been studied and TiO_2 and SiO_2 have been chosen as the layer materials. “Optilayer” and “Mcalc” softwares have been used to detect the layer numbers and optimum layer thicknesses.

Before the production of filters, high vacuum coating techniques have been studied to produce the most accurate production. At the end, electron beam deposition with plasma ion assisted deposition technique has been chosen and the coating system of SyrusPro1110 model of Leybold brand has been used for all the productions. Perkin Elmer Lambda 950 model spectrophotometer has been used for measuring the transmission and reflection spectrums.

For the production, two different designs have been done. First one has 27 layer and 2008.3 nm physical thickness. One the other hand, second one has 31 layer and 2377 nm physical thickness. When the first production has been done quartz crystal measuring unit has been chosen and optical monitoring system has been chosen for the second production. Moreover, backside antireflective coating design that has five layers and 652.2 nm physical thickness has been done and it has been also coated on the backside of the both productions. As a result, when we make a table that shows the physical properties of the filters we obtain tha data as shown on the Tables 5.1 and 5.2.

As a result, designed 27 layer NIR filter has been produced with a $\sim$ %2 transmission difference in the 720-1400nm spectral region and $\sim$ %0.9 transmission difference in the 400-680nm spectral region. Also, designed 31 layer NIR filter has been produced with a $\sim$ %1 transmission difference in the 720-1400nm spectral region and $\sim$ %0.8 transmission differ-

ence in the 400-680nm spectral region. In the same way, reflection difference is lower than %3 between designed and produced 27 layer NIR filters. For the 31 layer NIR filters reflection difference is lower than %2 for designed and produced filters. In conclusion, both theoretical and experimental studies performed throughout this work has enables us to design and produce a multilayer Near infrared interference filter that blocks the spectrum range of 400-700nm and transmits the spectrum range of 700-1400nm.

Table 5.1: Transmission and thickness values of produced and designed NIR interference filters.

Filter		**Substrate Positions**	**400-680 nm %T**	**720-1400 nm %T**	**Theoretical Value for 400-680 nm**	**Theoretical Value for 720-1400 nm**	**Theoretical Thickness**
27 layer NIR filter	Without Backside AR Coating	Positions-2	1.5	93.3	1.4	95.1	2008.3nm
		Positions-5	1.7	93.0			
		Positions-8	2.5	92.8			
	With Backside AR Coating	Positions-2	1.7	95.9	1.4	98.5	(2008.3 +652.2)nm
		Positions-5	2.2	95.6			
		Positions-8	2.0	95.7			
31 layer NIR filter	Without Backside AR Coating	Positions-2	1.8	94.1	0.8	95.0	2377nm
		Positions-5	1.5	94.2			
		Positions-8	1.6	94.3			
	With Backside AR Coating	Positions-2	2.2	97.2	0.8	98.4	(2377 +652.2)nm
		Positions-5	1.4	97.1			
		Positions-8	1.9	97.1			

Table 5.2: Reflection and thickness values of produced and designed NIR interference filters.

Filter		**Substrate Positions**	**400-680 nm %R**	**720-1400 nm %R**	**Theoretical Value for 400-680 nm**	**Theoretical Value for 720-1400 nm**	**Theoretical Thickness**
27 layer NIR filter	Without Backside AR Coating	Positions-2	95.2	4.9	98.3	4.6	2008.3nm
		Positions-5	96.5	5.3			
		Positions-8	97.4	4.7			
	With Backside AR Coating	Positions-2	95.8	3.3	98.3	1.6	(2008.3 +652.2)nm
		Positions-5	96.4	3.6			
		Positions-8	97.5	3.2			
31 layer NIR filter	Without Backside AR Coating	Positions-2	97.7	5.5	99.1	4.7	2377nm
		Positions-5	98.0	5.5			
		Positions-8	97.9	5.9			
	With Backside AR Coating	Positions-2	97.3	2.2	99.1	1.3	(2377 +652.2)nm
		Positions-5	97.3	2.2			
		Positions-8	97.8	2.4			

REFERENCES

[1] Optical Filters , www.rp-photonics.com/optical_filters.html , last visited on January 23 2012 .

[2] Donald M.Mattox , *Handbook Of Physical Vapor Deposition* . New Jersey, U.S.A., 1998.

[3] H.A. Macleod , *In Applied Optics and Optical Engineering* . Academic Press, New York, 1987.

[4] F. L. Pedrotti and L. S.Pedrotti , *Introduction to Optics*. Prentice-Hall, U.S.A., Second Edition, 1993.

[5] L.F. Drummeter and G.Hass, *Solar Absorbtance and Thermal Emitance of Evaporated Coatings* in G.Hass and R.E. Thun (eds .), Physics of Thin Films,Academic Press, New York, 1964, vol.2

[6] Smith J. W., *Modern Optical Engineering* . McGraw-Hill, New York, 2000.

[7] Wilson R.N., *Reflecting Telescope Optics II*. Springer, 1999.

[8] Eroglu C. *Design of Reflective and Antireflective Coatings for Space Applications* . Ms.Thesis, 2009.

[9] Ohring Milton, *Material Science of Thin Films*. AcademicPress, New York, 1992.

[10] Optical Coatings, www.cvimellesgriot.com/Products/Documents/TechnicalGuide/Optical-Coatings.pdf, last visited on January 23 2012.

[11] Thin Film Deposition, http://www.mrsec.harvard.edu/education/ap298r2004/Erli%20chenFabrication%20II%20-%20Deposition-1.pdf. 4/12/2004.

[12] Peter M. Martin, *Handbook of deposition Technologies for Films and Coatings*. Washington, 2009.

[13] H.A. Macleod, *Thin-film optical filters* . New York, 2001.

[14] Optical Coating Systems, www.leyboldoptics.com, last visited on January 23 2012 .

APPENDIX A

THICKNESS DATA FOR THE PRODUCED FILTERS

Table A.1: Thickness data for the produced 27 layer NIR interference filters

Physical Thickness (nm)	Optical Thickness (nm)	FWOT	QWOT	Material
85.54	125.74	0.13	0.5	L
25.67	58.85	0.06	0.24	H
101.31	148.92	0.15	0.6	L
42.2	96.76	0.1	0.39	H
61.87	90.95	0.09	0.36	L
42.68	97.87	0.1	0.39	H
68.65	100.91	0.1	0.4	L
53.27	122.15	0.12	0.49	H
89.98	132.26	0.13	0.53	L
44.86	102.86	0.1	0.41	H
73.55	108.11	0.11	0.43	L
33.78	77.45	0.08	0.31	H
73.6	108.19	0.11	0.43	L
55.89	128.14	0.13	0.51	H
89.07	130.93	0.13	0.52	L
62.22	142.67	0.14	0.57	H
106.91	157.14	0.16	0.63	L
59.32	136.01	0.14	0.54	H
97.16	142.82	0.14	0.57	L
69.98	160.45	0.16	0.64	H
100.34	147.48	0.15	0.59	L
54.5	124.97	0.12	0.5	H
111.72	164.22	0.16	0.66	L
72.24	165.64	0.17	0.66	H
62.11	91.29	0.09	0.37	L
74.29	170.33	0.17	0.68	H
195.62	287.55	0.29	1.15	L

Table A.2: Thickness data for the produced 31 layer NIR interference filters

Physical Thickness (nm)	Optical Thickness (nm)	FWOT	QWOT	Material
105.49	156.35	0.31	1.25	L
25.91	6269	0.13	0.5	H
114.39	16954	0.34	1.36	L
61.69	149.26	0.3	1.19	H
78.89	116.92	0.23	0.94	L
75.81	183.42	0.37	1.47	H
97.77	144.91	0.29	1.16	L
55.21	133.57	0.27	1.07	H
117.84	174.64	0.35	1.4	L
62.56	151.35	0.3	1.21	H
92.66	137.33	0.27	1.1	L
68.47	165.67	0.33	1.33	H
105.59	156.49	0.31	1.25	L
59.55	144.09	0.29	1.15	H
95.09	140.93	0.28	1.13	L
73.06	176.78	0.35	1.41	H
84.71	125.54	0.25	1.0	L
52.36	126.67	0.25	1.01	H
84.74	125.58	0.25	1.0	L
32.47	78.55	0.16	0.63	H
72.05	106.78	0.21	0.85	L
50.3	121.69	0.24	0.97	H
82.09	121.66	0.24	0.97	L
48.62	117.63	0.24	0.94	H
85.69	127	0.25	1.02	L
30.03	72.65	0.15	0.58	H
78.56	116.43	0.23	0.93	L
52.34	126.63	0.25	1.01	H
70.1	103.9	0.21	0.83	L
60.55	146.51	0.29	1.17	H
197.82	293.19	0.59	2.35	L

Table A.3: Thickness data of antireflective backside coating for the produced filters

Physical Thickness (nm)	**Optical Thickness (nm)**	**FWOT**	**QWOT**	**Material**
185.33	272.42	0.272	1.09	L
30.56	70.06	0.07	0.28	H
55.97	82.28	0.082	0.329	L
218.82	501.73	0.501	2.007	H
161.53	237.44	0.237	0.95	L